Swing up Control of an Inverted Pendulum

Master Thesis
Group 1034

Aalborg University
Electronics and IT

All the simulations and data analysis in this project have been done using Matlab 2016a. Images have been treated with Inkscape 0.91. For Arduino implementation has been used Arduino 1.6.7.

Title:
Swinging up Control of an Inverted Pendulum

Theme:
Scientific Theme

Project Period:
Master Thesis

Project Group:
1034

Participant(s):
Ioannis Kapnisakis
Francesco Catarinacci

Supervisor(s):
Palle Andersen
John-Josef Leth

Copies: 3

Page Numbers: 77

Date of Completion:
October 31, 2016

Abstract:

This project proposes a strategy to swing up and control an inverted pendulum around the upright position. Electrical and mechanical parts have been analysed and the mathematical model of the system has been developed. The methodology proposed performs a swing up algorithm based on the total energy of the inverted pendulum, switching then to al linear controller that stabilises the pendulum upright. Simulation are performed to test the system behaviour while the designed control algorithm is applied. Experimental results of the implementation in the real system are also presented. Finally, an optimization approach has been performed by implementing off-line an extended Kalman filter.

Contents

Preface

This paper contains a collection of worksheets for a master thesis conducted by students of Electronics and IT at Aalborg University. The report consists of 7 chapters and describes the concepts related to the non linear control of an inverted pendulum.

References appearing in the report are collected in a source list at the end of the report. The references are organized using the numbering method, so the reference in the text is made by a [Number] which leads to the source list in where books and articles are listed by author, title, publisher. Internet sites are indicated by URL, author (if provided), title page.

Figures and tables are numbered according to the chapter , for example the first figure in chapter 5 has the number 5.1, etc. Explanatory text for figures and tables can be found under the given figures and tables.

The paper comes with the attached CD containing data sheet and source code used in the project.

<div align="right">Aalborg University, October 31, 2016</div>

Ioannis Kapnisakis
<ikapni14@student.aau.dk>

Francesco Catarinacci
<fcatar15@student.aau.dk>

Chapter 1

Introduction

The objective of this chapter is to give an overview of the inverted pendulum system and its stabilization and optimization tasks, as well as a description of each part of the studied system.

The Inverted Pendulum Structure

Inverted pendulum systems are a classic control theory problem and many different versions of it exist. In this report has been considered, among the most familiar types, the cart inverted pendulum. This type of system consists of three basic elements:

- A slid consisting of two parallel rails;

- A cart moving horizontally along the sled;

- A rotating single-arm pendulum, mounted on the cart.
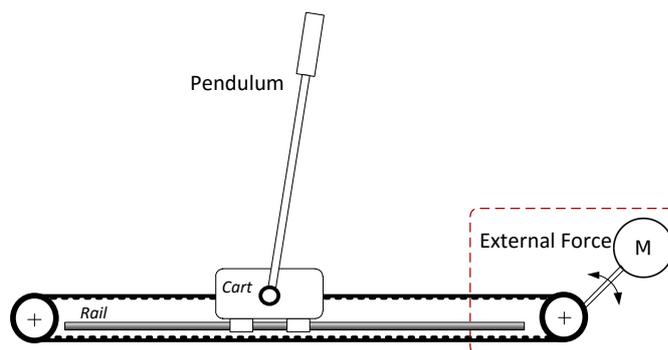
Figure 1.1: System setup

When the bob stands in the upright position, the system is in an unstable equilibrium. Therefore, it naturally tends to fall over in the downward position swinging back and forth. To bring the pendulum upright and maintain it there, a stabilizing action is performed by an external force acting on the cart. The actual system is then composed by the cart pendulum system itself and a subsystem controlling the given input force. Setup has two degree of freedom: the horizontally movement of the cart on a sled and the rotation of the pendulum rod. The cart can be directly driven back and forth by the actuator, while the pendulum can freely rotate around its axis.

Project Background

Since 1960s, this kind of systems are used to explain ideas in linear control. By means of their nonlinear nature, from 1990s, pendulums continued to be used to illustrate ideas in nonlinear control domain such as passivity based control, backstepping or nonlinear model reduction as well as task oriented control as swinging up [18]. Among the different controlling approaches present in the literature, those considered more relevant writing this report are shown below. Wei et al. [20] proposed a swing up strategy when the cart has a restricted horizontal travel. Chung and Hausen [5] presented a control law to swing up considering the energy of the pendulum while regulating the cart position. Spong and Praly [17] proposed a swing up where in the stability analysis is taken into account the Lyapunov theory. Fantoni and Lozano [7], inspired by [17], presented an approach where the total energy of the inverted pendulum is considered in the control algorithm. Issues due to the friction in the pendulum, not considered in [7], have been contemplate by Ishitobi et al. [9]. For theoretical concepts allover the report, has been essential the work of Kahlil [12].

Problem Statement

The main focus of this project is to develop and apply a control strategy to swing up the pendulum and then stabilize it in the upright vertical position. An energy control strategy is applied for this purpose. Close to the unstable point, pendulum is kept standing by means of changing the controller from the non linear to a linear one. Modifications are applied to the original non linear controller due to issues caused by frictions and singularities. Then, an extended Kalman filter is introduced to obtain a better estimation of the states.

The objectives of this project are expected to address the following points:

- **Detailed description** of electrical and mechanical parts of the system

- **Develop and simulate** a stabilizing non-linear control strategy for the system model

- **Develop and simulate** an extended Kalman filter to remove uncertainties in the states estimations

- **System Analysis** of the controller on the real system in the laboratory facilities.

Overview This paper is organized as follows: In **Chapter Two** the description of the system is given; in **Chapter Three** the mathematical model of the system is shown; in **Chapter Four** the energy control method is presented and the problem of Lyapunov function is discussed. Moreover the complete control law is designed and simulations using Matlab are shown, while in **Chapter Five** the laboratory implementation is presented. In **Chapter Six** an extended Kalman filter is designed and applied to the system. Finally, **Chapter Seven** is devoted to presenting the conclusions.

Chapter 2

System Description

Introduction

Input force to move the *inverted pendulum* is provided from a *DC motor* (the actuator) through a belt; pendulum cart system's outputs are cart horizontal position and pendulum angular position. An *encoder* mounted on the actuator measures the cart displacement, while another encoder measures the pendulum leaning. DC motor is piloted by the current coming from a *pulsed power amplifier* (*servoamplifier*) according to the voltage reference sent from a *microcontroller* board. Measurements received from the encoders are used by the microcontroller to set the reference. The setup is connected to a PC via an USB-port: the program to run the setup is loaded to the microcontroller and measured data are then sent back to the PC. Components of the overall system are illustrated in figure 2.1 and described in the following sections.
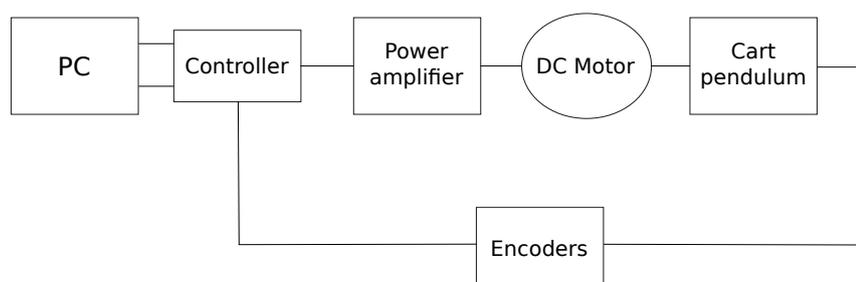
Figure 2.1: Block diagram of the laboratory setup

Microcontroller board

In the studied setup, an Arduino Due board [1] is used to implement the designed controller. Arduino consists of both a physical programmable board and a

software, called IDE (Integrated Development Environment), used to program the board. It allows to write programs, read sensors and control motors. The Arduino Due board:

- features an Atmel SAM3X8E ARM Cortex-M3 CPU microcontroller;

- operates at 3.3[V], unlike other commonly used Arduino boards operating at 5[V];

- stores programs in the available 512 [KB]of RAM;

- executes many hundred thousands lines of C code per second having a clock speed of 84 [MHz];

- presents a micro-USB port to be connected to a computer;

- can be connected with a battery or an AC-to-DC adapter, when more power is required.

- has 54 digital input/output pins;

- owns 12 analog input pins;

- carries 2 DAC (digital to analog) pins providing analog output with 12-bit resolution (4096 levels).

Real DAC output range is only from 0.55[V] to 2.75[V]: output current from those pins is not enough to run a motor directly (the one used in this project has a nominal voltage of 48[V] and a nominal current of 4.58[A]), with the result of damaging the board. Other boards can be fitted on top of Arduino to provide additional capabilities.
Therefore, to obtain a reference voltage enough to drive the motor, an interface of a *shield* and a *voltage amplifier* ($-10[V], +10[V]$) is used. In this way a reference voltage is sent to a power amplifier which eventually supplies and drives the dc motor with its nominal values.

As any automatic system, tasks in the Arduino board can be divided in three main parts: *Signal Inputs*, *Software Decisions* and *Signal Outputs*. In this project they are described as follows:

- Inputs (cart position and pendulum angular position) are sent by two encoders to digital pins.They are read as bytes and converted to integers using an embedded library.

- Once inputs arrive, the controller in Arduino computes the suitable input to reach the setpoint.

- Output is sent to a Digital to Analog pin (DAC0): it sets the voltage reference for the power amplifier.

Arduino IDE   The Arduino Integrated Development Environment is the software used to write the code for the Arduino board. Software libraries are used to maintain the main code simple. A brief description of those libraries used in this project follows:

- *Joint library* manages data coming from the encoders. It also estimates the cart velocity from its position and compensates Coulomb and linear viscous frictions;

- *looptime library*;

- *Utility library* defines functions `sign` and `saturation`.

Servoamplifier

A reference signal is set by an Arduino board. This signal is adapted with a servoamplifier (Maxon 4-Q-DC ADS 50/10) [13] to drive the DC motor accordingly. Moreover, the servoamplifier sets the reference to be given to the DC motor, which aims to control the current in the motor. Hence controlling its speed and torque.

Accordingly, the mechanical torque (T_M) of the DC motor results:

$$T_M = k_M * I_M \tag{2.1}$$

where k_M is the torque constant of the motor defined in [14] and I_M is the motor current.

DC Motor

The DC motor Maxon 370356 RE 50, $200W$ [14] is a permanent magnet motor which moves the cart of the inverted pendulum system. The supplied voltage (V_a) of the motor armature corresponds to the motor current I_M that flows inside the armature. The DC motor converts this electrical current to a mechanical torque T_M according to (2.1) that characterizes the motion of the motor shaft. The electrical diagram of the used DC motor is shown in figure 2.2.
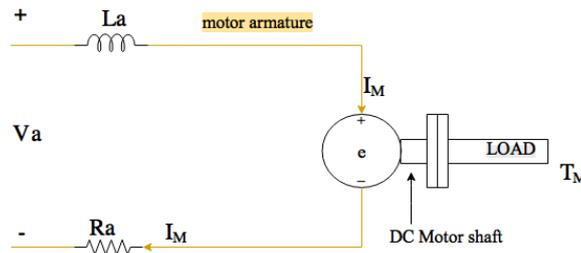
Figure 2.2: Electrical circuit of the DC motor

The armature of the motor is characterized by a resistance R_a and an inductance L_a. In general, during the operation of a DC motor:

- The current I_M flows in presence of the magnetic field and produces the rotation of a shaft which is connected with the armature.

- The armature-shaft is attached to a load to which is applied the mechanical torque T_M of the motor.

An opposite electromotive force (back-electromotive-force, EMF) e is produced due to the changes of the magnetic field that passes through the armature.

Cart Pendulum

The cart pendulum structure is the mechanical part of the investigated system. As it has been described in section 1.1 this structure consist of an aluminium rail, a cart that slides on it as well as a rotating pendulum attached on the cart. Through the horizontal back and forth motion of the cart, the pendulum rotates accordingly. Cart is belt driven from a controlled DC motor, while the pendulum is actuated from the cart. The rotational axis of the cart is attached on the shaft of a second non functional DC motor. Such a structure is convenient to implement the sensor for the pendulum feedback signals.

Encoders

During the control procedure of the system, feedback signals for the position of the cart and pendulum are needed. Therefore, two rotary encoders, AVAGO HEDS-5540 [2], are used to obtain the positions feedback for the cart and pendulum. The encoders are attached to the driven motors of the cart and pendulum. The DC motor attached on pendulum rotational axis is not used and not controlled in the present application.

Figure 2.3 shows the main parts of an optical incremental encoder. A light source (LED diode) sends a light beam which passes through a disc plate that is attached in the DC motor shaft.
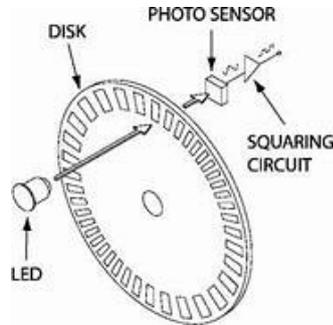
Figure 2.3: A simplified structure of the optical incremental encoder [16].

This plate has spaced dark and transparent segments on its surface that forms a simple radial pattern for the angular position of the shaft. The load to be measured is connected in the shaft of the encoder. With the shaft rotation, a series of light exposures is created which is tracked by a photo sensor (detector).

More specifically, the disc plate contains a grid diaphragm which split the incident light beam into a second beam of light 90° out of phase. In this way two outputs from the sensing channels A and B are produced whose phase difference (90°) is used to define the rotational direction of the shaft. Afterwards, the beams A and B are received by two separate photo detector components and are transformed into two square wave signals via a signal processor. This processor analyses the signals to obtain the position information. Figure 2.4 demonstrates the square waves that are exported from an encoder for different rotations of its shaft.
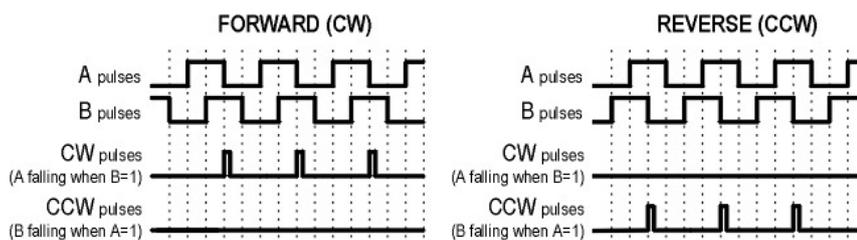
Figure 2.4: The produced quadrature signals of the optical encoder.

Resolution is a characteristic of an optical encoder that is considered according to the field of implementation of the encoder. For the incremental rotary encoders it is defined as counts per revolution. The resolution of the encoder is related with the segments (the transparent and black segments) of the disk plate and is one of

the characteristics that define the performance of the encoder. The used encoders, AVAGO HEDS-5540 [2], have a high resolution, that is 1024 counts per revolution. For the measurement of the pendulum displacement this resolution is expressed in *radians/count* while for the cart displacement in *meters/count*.

Information related with the resolution of the used encoders can be found in the Arduino library `joint.cpp` that includes the algorithm for the estimation of angular and linear displacement of the system by differentiating the position measurements. The available information which are used to define the resolution of encoders are:

Length of the sled where the cart moves	$0.769[m]$
Pendulum displacement per revolution	$2\pi[rad]$
Total counts within the overall length of sled	8737
Total counts per pendulum revolution	2000

the resolutions for the used encoders are defined as:

- $Res_{cart} = \frac{0.769[m]}{8737counts} = 8 * 10^{-6}[m]/count$ the resolution of the encoder that measures the cart displacement

- $Res_{pen} = \frac{2\pi[rad]}{2000counts} = 0.0031[rad]/count$ or $0.18[degrees]/count$ the resolution of the encoder that measures the pendulum displacement

In combination with the small sampling time ($T_s = 0.005[s]$) of the Arduino board microprocessor a quite good measurements for the cart and the pendulum displacements of the system is obtained. However, these resolutions that define the quantization error of the encoders can introduce a small measurement uncertainty. This small uncertainty is considered in Chapter 6 where an EKF is designed for the inverted pendulum system.

Chapter 3

System Dynamics

Introduction

The purpose of this chapter is to present a formulation of the mathematical model of the system. One of the objectives in this thesis, is the development of a proper control strategy such that the system has a desired behaviour. A proper mathematical model is required for the design of this control. As previously mentioned, an inverted pendulum is under investigation. The physical system available at AAU laboratory facilities consists mainly of two subsystems:

- **The electrical subsystem** which creates a desired force according to a reference

- **The mechanical subsystem** that receives this force
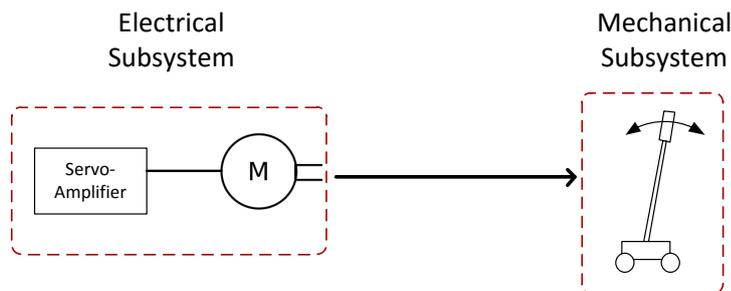
Figure 3.1: Electrical and Mechanical Subsystems

In figure 3.1, these parts of the studied physical system are shown, while in Chapter 2 are described briefly. For both subsystems a dynamical analysis is performed. In this way it is expected the development of a mathematical model that represents the real system in a large extend. Consequently, the applied control

in the system can be designed with more accuracy. In the following sections, a dynamical analysis for the components included in each subsystem is presented. Finally, the response of these two subsystems is compared.

Electrical Subsystem

The electrical subsystem consists of a power amplifier and a DC motor. These dynamics are combined such that to formulate the electrical subsystem dynamics.

Power Amplifier Dynamics

Internally, the servoamplifier performs a current control whose purpose is to make the actual current I_M to follow a reference a value. This is ensured through a high gain β in the current feedback. Afterwards the error signal is amplified and the controlled current I_M that supplies the DC motor is obtained as shows figure 3.2.
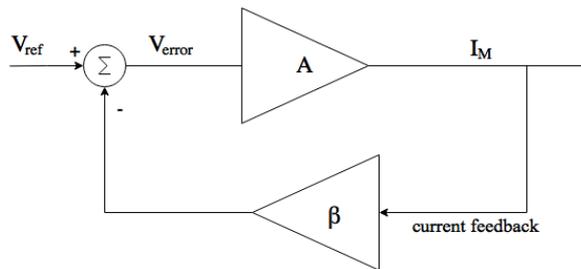
Figure 3.2: Simplified schematic diagram of the servoamplifier.

With the block A is represented the open loop gain while with β the feedback gain which is applied in the signal I_M.

DC Motor Dynamics

The electric circuit of the DC motor (figure 2.2) is characterized by

$$V_a(t) = L_a \frac{dI_M}{dt} + R_a I_M + e \tag{3.1}$$

which represents the supplied voltage to the motor armature including the back EMF voltage e [Zaccarian].

This voltage e is considered as a disturbance during the operation of the DC motor. By Laplace transformation of (3.1) it is obtained the current $I_M(s)$ that flows in the motor.

$$I_M(s) = \frac{\frac{1}{R_a}}{1 + \frac{L_a}{R_a}s}(V_a(s) - e(s)) \tag{3.2}$$

and

$$\frac{I_M(s)}{V_a(s) - e(s)} = \frac{\frac{1}{R_a}}{\frac{L_A}{R_a}s + 1} = \frac{K_a}{\tau s + 1} \tag{3.3}$$

that express the transfer function of the motor circuit (figure 2.2), as a first order system. Term $K_a = \frac{1}{R_a}$ is the motor gain and $\tau_a = \frac{L_a}{R_a}$ the time constant of the motor. In the following section, the dynamical response of the DC motor will be investigated in order to see if the electrical dynamics should be considered when studying the inverted pendulum.

Power Amplifier-DC Motor Subsystem Dynamics

The response of the inverted pendulum is defined from the operational behaviour of all the components that are included in the system. The DC motor that moves the pendulum cart consists of some mechanical parts whose operation may affect the response and consequently the satisfactory control of the inverted pendulum. Power electronic components included in the servoamplifier to regulate the motor current I_M, with their operational characteristics, might have an influence in the response of the overall system. Therefore, the dynamical response of the servoamplifier-DC motor subsystem has been investigated. Ideally, it should be much faster compared with the response of the inverted pendulum such that to not have any influence in the control of the system.

Figure 3.3 shows the generalized block diagram of the servoamplifier in connection with the DC motor. For the present analysis the function of the servoamplifier has been considered as a simple and fast enough amplification of the processed signals through the gains A and β, while the block H represents the transfer function of the motor (2.2). The back electromotive voltage e that is generated during the operation of the DC motor is considered as a disturbance in this subsystem. To simplify the dynamical analysis, the effect of the voltage e is ignored.

As it is referred in section 2.3 the servoamplifier performs a current control such that to keep the motor current I_M close to a reference value that is set in the Arduino board. The transfer function of the closed loop system in figure 3.3 is defined as:

$$\frac{I_M}{V_{ref}} = \frac{A * H}{1 + \beta * A * H} \tag{3.4}$$
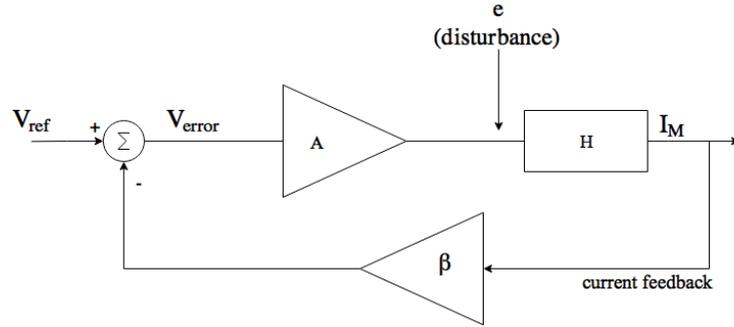
Figure 3.3: Simplified diagram of the servoamplifier connected with the electrical part of the dc motor

Substituting (3.3) in (3.4) it is obtained:

$$\frac{I_M}{V_{ref}} = \frac{A\frac{\frac{1}{R_a}}{\frac{L_a}{R_a}s+1}}{1+\beta A\frac{\frac{1}{R_a}}{\frac{L_a}{R_a}s+1}} = \frac{\frac{\frac{A}{R_a}}{\frac{L_a}{R_a}s+1}}{\frac{\frac{L_a}{R_a}s+1+\beta A\frac{1}{R_a}}{\frac{L_a}{R_a}s+1}} = \frac{\frac{A}{R_a}}{\frac{L_a}{R_a}s+\beta A\frac{1}{R_a}+1} \tag{3.5}$$

which is brought in the form of the transfer function of a first order system, dividing the nominator and denominator of (3.5) with $\frac{1}{\frac{\beta A}{R_a}+1}$

$$\frac{I_M}{V_{ref}} = \frac{\frac{A}{R_a(\frac{\beta A}{R_a}+1)}}{\frac{L_a}{R_a(\frac{\beta A}{R_a}+1)}s+1} \tag{3.6}$$

With the aim of a small current error between the current flowing inside the motor (I_M) and the reference signal, gain (β) in the servoamplifier is assumed high enough. This results to:

$$R_a(\frac{\beta A}{R_a}+1) \approx \beta A \tag{3.7}$$

Thus, considering (3.7), equation (3.6) is approximated as:

$$\frac{I_M}{V_{ref}} \approx \frac{\frac{1}{\beta}}{\frac{L_a}{\beta A}s+1} \tag{3.8}$$

which expresses the first order subsystem of the servoamplifier-DC motor with time constant $\tau_{SaM} = \frac{L_a}{\beta A}$ and dc-gain $K_{SaM} = \frac{1}{\beta}$.
By observation of the subsystem response, characteristics τ_{SaM} and K_{SaM} have been estimated. A square wave has been generated with the purpose to move the cart on the sled back and forth with a force of 1[N]. A corresponding voltage $V_{ref} = 33.3051mV$ has been measured as output from the microcontroller. So,

generating a square wave of peak amplitude $V_{ref} = 33.3051mV$ within a period of $T = 1.2[s]$, the motor current input I_M has been measured with a current probe and an oscilloscope. As it can be seen in figure 3.4, the received signal (blue) is very noisy due to the motor ripples. To estimate gain K_{SaM}, mean values ($\pm1.43[A]$) of the square wave response are been considered.
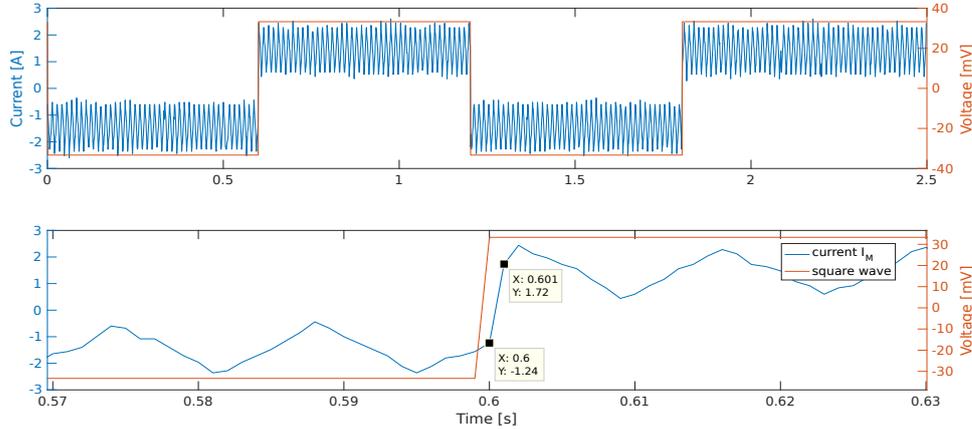
Figure 3.4: Response of the servoamplifier-dc motor system (top) with the zoomed area of interest (bottom).

The resolution of oscilloscope is 0.001 [s]: the zoom in figure 3.4 shows that within a sample time step (from $t = 0.599[s]$ to $t = 0.6[s]$), the input pulse switches from $-30.3051[V]$ to $+30.3051[V]$ and current I_M is almost as fast as the input. Estimation of the time constant can not be then obtained by computation. Even though, in the worst case, it could be considered equal to the resolution step, it has been assumed to evaluate the time constant as 10 times faster. Summarizing, multiplying the motor's input current by the sensitivity of the probe it is obtained:

$$V_M = \pm1.43[A] * 100[mV/A] = \pm143[mV] \tag{3.9}$$

Consequently,

$$K_{SaM} = \frac{143[mV]}{33.3051[mV]} = 4.2936 \tag{3.10}$$

while

$$\tau_{SaM} = 0.0001[s]. \tag{3.11}$$

Substituting (3.10) and (3.11) in (3.8) is obtained the transfer function of the servoamplifier-DC motor system in the Laplace domain:

$$\frac{I_M}{V_{ref}} = \frac{4.2936}{0.0001s + 1} \tag{3.12}$$

Mechanical Subsystem

In this section, the mathematical model of the inverted pendulum presented in figure 3.5 is obtained from the Euler-Lagrangian equation, based on the energy of the system. A more detailed description of the system model formulation is presented in [4].
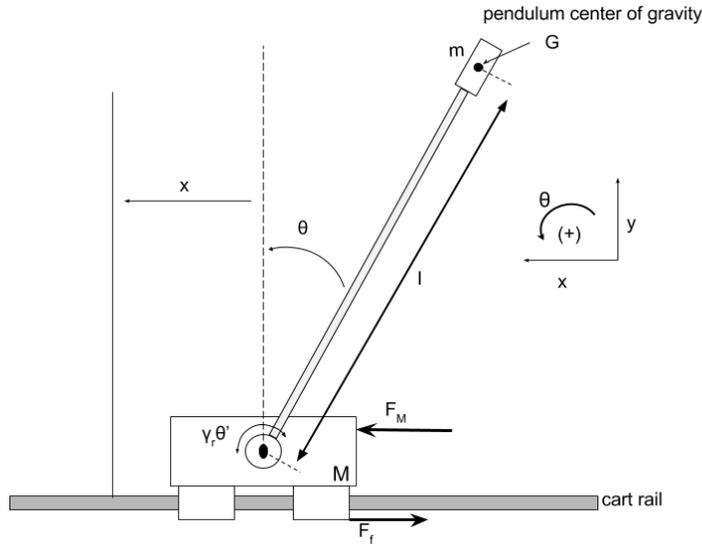
Figure 3.5: Set up of the mechanical subsystem of the inverted pendulum

The mass of the pendulum rod (l) is considered neglectable, while the attached mass (m) at the end of the pendulum rod is considered a point mass. Therefore, the pendulum centre of gravity (G) is placed in the geometrical centre of the mass (m) and its position is defined by

$$x_G = x + l sin\theta$$
$$y_G = l cos\theta \tag{3.13}$$

The differential equations of motion of the inverted pendulum are derived from the Euler Lagrangian equations

$$\frac{d}{dt}\left(\frac{\partial L}{\partial \dot{q}}(q,\dot{q})\right) - \frac{\partial L}{\partial q}(q,\dot{q}) = \tau$$

where $q = (q_1 \ldots q_n)^T$ represents the generalized coordinates of the system and $\tau = (\tau_1 \ldots \tau_n)^T$ defines the external as well as the non conservative (friction) forces that

are applied to the system. The Lagrangian function L is defined as the difference of kinetic (K) and potential (P) energy of the system ($L = K - P$).

Firstly, the kinetic and potential energies of the system used in the Lagrangian formulation are defined. Both cart and pendulum have kinetic energy and thus, considering the pendulum in figure 3.5, the total kinetic energy of the system is

$$
\begin{aligned}
K &= K_{cart} + K_{pen} \\
&= \frac{1}{2}M\dot{x}^2 + \frac{1}{2}m\left(\frac{d}{dt}(x + l\sin\theta)\right)^2 + \frac{1}{2}m\left(\frac{d}{dt}(l\cos\theta)\right)^2 \\
&= \frac{1}{2}(M+m)\dot{x}^2 + ml\dot{x}\dot{\theta}\cos\theta + \frac{1}{2}ml^2\dot{\theta}^2
\end{aligned}
$$

and the potential energy

$$
P = mglcos(\theta - 1)
$$

is defined only from the pendulum position, since the cart moves only horizontally. Secondly, the Lagrangian function is given by

$$
\begin{aligned}
L &= K - P \\
&= \frac{1}{2}(M+m)\dot{x}^2 + ml\dot{x}\dot{\theta}\cos\theta + \frac{1}{2}ml^2\dot{\theta}^2 - mgl\cos\theta. \quad\quad (3.14)
\end{aligned}
$$

In the cart pendulum system, the chosen coordinates are the cart (x) and the pendulum (θ) displacement, which leads to the following Euler-Lagrangian equation with the corresponding partial derivatives:

$$
\frac{d}{dt}\left(\frac{\partial L}{\partial \dot{x}}\right) - \frac{\partial L}{\partial x} = \tau_1
$$

$$
\frac{d}{dt}\left(\frac{\partial L}{\partial \dot{\theta}}\right) - \frac{\partial L}{\partial \theta} = \tau_2. \quad\quad (3.15)
$$

Since the Lagrangian function L does not depend on x, it follows

$$
\frac{\partial L}{\partial x} = 0
$$

while

$$
\begin{aligned}
\frac{d}{dt}\left(\frac{\partial L}{\partial \dot{x}}\right) &= \frac{d}{dt}\left((M+m)\dot{x} + ml\dot{\theta}\cos\theta\right) \\
&= (M+m)\ddot{x} + ml\ddot{\theta}\cos\theta - ml\dot{\theta}^2\sin\theta. \quad\quad (3.16)
\end{aligned}
$$

For the θ coordinate

$$
\frac{\partial L}{\partial \theta} = -ml\dot{x}\dot{\theta}\sin\theta + mgl\sin\theta
$$

and

$$\frac{\partial L}{\partial \dot{\theta}} = ml\dot{x}\cos\theta + ml^2\dot{\theta}$$

that gives

$$\frac{d}{dt}\left(\frac{\partial L}{\partial \dot{\theta}}\right) - \frac{\partial L}{\partial \theta} = ml\ddot{x}\cos\theta + ml^2\ddot{\theta} - mgl\sin\theta. \tag{3.17}$$

Friction is the non conservative force of the system. Both, Coulomb and viscous friction are defined as: $F_c sign(\dot{x}) + \gamma\dot{x}$ for the cart, while only viscous friction is considered in the pendulum: $\gamma_r\dot{\theta}$. From this point, Coulomb friction force $F_c sign(\dot{x})$ is referred as F_c for simplicity.

Combining also the control input (F_M) that is applied to the cart, the external forces which are implemented in the system are:

$$\tau_1 = F_M - F_c - \gamma\dot{x} \tag{3.18}$$

$$\tau_2 = -\gamma_r\dot{\theta} \tag{3.19}$$

Substituting (3.16), (3.17) and (3.18), (3.19) in (3.15) the model of the cart pendulum system is obtained as

$$(M + m)\ddot{x} - ml\dot{\theta}^2\sin\theta + ml\ddot{\theta}\cos\theta = F_M - F_c - \gamma\dot{x} \tag{3.20a}$$
$$ml^2\ddot{\theta} - mgl\sin\theta + ml\cos\theta\ddot{x} = -\gamma_r\dot{\theta} \tag{3.20b}$$

where F_M is the controlled applied force from the DC motor that moves the cart. From now on, the input force will be referred as a unique term $u = F_M - F_c$, since Coulomb friction is compensated by software.

System parameters contained in model (3.20) were estimated through experimental processes conducted with the available inverted pendulum system located in the laboratory facilities of AAU. In Appendix A, the used estimation methods as well as the values of the estimated parameters are presented. For this reason, through the report any reference to the system parameters is related with the content of Appendix A.

Response Comparison of Electrical and Mechanical Subsystem

This section presents a dynamical analysis of the previous referred subsystems, as well as the comparison between the response behaviour of both subsystems.

A demanding point during the control of the system is when the pendulum is close to the upright vertical position and should be stabilized there via a linear

controller. At this point the motor, driven from the servoamplifier, should respond much faster compared with the inverted pendulum response. The comparison between the response time of the linearised inverted pendulum [4] and the response time of the servoamplifier-DC motor system is based on the position of the poles of each system. Figure 3.6 shows the system (3.12) pole (blue one) to be very far on the left with respect to the linearised inverted pendulum system poles (red ones).
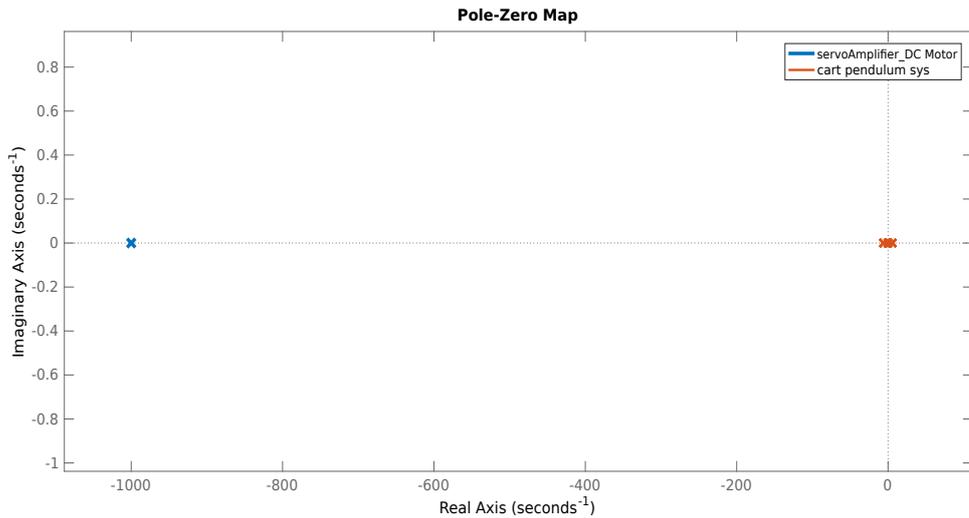
Figure 3.6: Pole location for the linearized inverted pendulum and the servoamplifier-DC motor system.

It can be clearly seen that the subsystem of the servoamplifier-DC motor responds much faster than the overall system. Therefore, the control of the inverted pendulum can be assumed to be not affected from the electrical subsystem. Consequently, the control design will be based on the mechanical subsystem dynamics (3.3).

The Underactuated System of Cart Pendulum

In this section, nonlinear state equations for the cart pendulum system are derived from the state space form.

A general form of a second order controllable dynamical system is:

$$\ddot{q} = f_1(q, \dot{q}) + f_2(q)u \tag{3.21}$$

where q is the state vector, $f_1(q, \dot{q})$ represents the system dynamics, $f_2(q)$ the input matrix and u the control vector. The inverted pendulum system is an underactuated mechanical system because its control actuators are less than the degrees of

freedom to be controlled. More specifically, the displacements of cart (x) and pendulum (θ) of the system are the parameters to be controlled. Using the generalized coordinate q, system (3.20) can be presented in the state space form:

$$\mathbf{M}(q)\ddot{q} + \mathbf{C}(q,\dot{q})\dot{q} + \mathbf{D}\dot{q} + G(q) = \tau \tag{3.22}$$

where

$$q = \begin{bmatrix} x \\ \theta \end{bmatrix}, \quad \mathbf{M}(q) = \begin{bmatrix} M+m & mlcos\theta \\ mlcos\theta & ml^2 \end{bmatrix} \tag{3.23}$$

$$\mathbf{C}(q,\dot{q}) = \begin{bmatrix} 0 & -mlsin\theta\dot{\theta} \\ 0 & 0 \end{bmatrix} \tag{3.24}$$

$$\mathbf{D} = \begin{bmatrix} \gamma & 0 \\ 0 & \gamma_r \end{bmatrix} \tag{3.25}$$

$$G(q) = \begin{bmatrix} 0 \\ -mgl\sin\theta \end{bmatrix}, \quad \tau = \begin{bmatrix} u \\ 0 \end{bmatrix} \tag{3.26}$$

Matrix $\mathbf{M}(q)$ is a symmetric inertia matrix with determinant

$$\det(\mathbf{M}(q)) = (M+m)ml^2 - m^2l^2\cos^2\theta$$
$$= ml^2(M+m\sin^2\theta) > 0 \tag{3.27}$$

that shows it is positive definite for all q. $\mathbf{C}(q,\dot{q})$ represents centrifugal and Coriolis forces. In term $\mathbf{D}$ there are viscous damping coefficients while $\mathbf{G}(q)$ accounts for gravitational forces and is given as the derivative with respect to q of the potential energy $P(q)$ [12]. Moreover, through equations (3.23), (3.24) is defined

$$\dot{\mathbf{M}}(q) - 2\mathbf{C}(q,\dot{q}) = \begin{bmatrix} 0 & ml\sin\theta\dot{\theta} \\ -ml\sin\theta\dot{\theta} & 0 \end{bmatrix} \tag{3.28}$$

that is a skew-symmetric matrix,that follows

$$z^T(\dot{\mathbf{M}}(q) - 2\mathbf{C}(q,\dot{q}))z = 0 \quad \forall z \in R^2 \tag{3.29}$$

Using the system (3.22) the term ($\ddot{q}$) can be obtained from

$$\ddot{q} = \mathbf{M}(q)^{-1}(-\mathbf{C}(q,\dot{q})\dot{q} - \mathbf{D}\dot{q} - G(q) + \tau)$$

The term $\mathbf{M}^{-1}$ can be attained using (3.23), (3.24), (3.27) and is defined as

$$\mathbf{M}^{-1} = \frac{1}{\det(\mathbf{M})}\begin{bmatrix} ml^2 & -ml\cos\theta \\ -ml\cos\theta & M+m \end{bmatrix}. \tag{3.30}$$

Thus, the non linear state space model is reached:

$$\begin{bmatrix} \ddot{x} \\ \ddot{\theta} \end{bmatrix} = \frac{1}{\det(\mathbf{M})} \begin{bmatrix} ml^2 & -ml\cos\theta \\ -ml\cos\theta & M+m \end{bmatrix} \begin{bmatrix} (-\mathbf{C}) \begin{bmatrix} \dot{x} \\ \dot{\theta} \end{bmatrix} + (-\mathbf{D}) \begin{bmatrix} \dot{x} \\ \dot{\theta} \end{bmatrix} + (-G) + \tau \end{bmatrix}$$

$$\begin{bmatrix} \ddot{x} \\ \ddot{\theta} \end{bmatrix} = \frac{1}{\det(\mathbf{M})} \left(\begin{bmatrix} 0 & m^2l^3\dot{\theta}sin\theta \\ 0 & -m^2l^2\dot{\theta}sin\theta cos\theta \end{bmatrix} \begin{bmatrix} \dot{x} \\ \dot{\theta} \end{bmatrix} + \begin{bmatrix} -m^2l^2g\sin\theta\cos\theta \\ (M+m)mgl\sin\theta \end{bmatrix} \right.$$
$$\left. + \begin{bmatrix} -ml^2\gamma & ml\cos\theta\gamma_r \\ ml\cos\theta\gamma & -(M+m)\gamma_r \end{bmatrix} \begin{bmatrix} \dot{x} \\ \dot{\theta} \end{bmatrix} + \begin{bmatrix} ml^2u \\ -ml\cos\theta u \end{bmatrix} \right) \quad (3.31)$$

which defines the state equations for $\ddot{x}$ and $\ddot{\theta}$:

$$\ddot{x} = \frac{msin\theta(l\dot{\theta}^2 - gcos\theta) - \gamma\dot{x} + \frac{\gamma_r cos\theta\dot{\theta}}{l} + u}{M + msin^2\theta} \quad (3.32)$$

$$\ddot{\theta} = \frac{-m^2l^2sin\theta cos\theta\dot{\theta}^2 + ml\gamma cos\theta\dot{x} - (M+m)\gamma_r\dot{\theta} + (M+m)gmlsin\theta - mlcos\theta u}{ml^2(M + msin^2\theta)}$$
$$(3.33)$$

The total energy of the system is studied in the following section. The various positions of the system correspond to different values of the total energy which will be a guideline for the formulation of the control law.

Chapter 4

Control Design

Introduction

This chapter deals with the design of a swing up strategy for the inverted pendulum. Initially, the cart pendulum system is presented in a state space form using generalized coordinates. Afterwards, the total energy of the system is defined. It is used in the formulation of the control law. Eventually, using LaSalle's invariance principle the control law is obtained. Related theorems and definitions are also referred.

Energetic Approach

To swing up the pendulum to the upright vertical position is used a strategy that controls the total amount of energy in the system: adding enough energy, the pendulum is swung up from the hanging position to its unstable equilibrium point. The total energy of the system $E(q, \dot{q})$ is defined as the sum of its kinetic ($K(q, \dot{q})$) and potential ($P(q)$) components. $P(q)$ has been initially chosen to be zero at the origin ($P(0) = 0$) but, because of conditions imposed on the derivative of the Lyapunov function, as described later in this chapter, an offset $P_{off} = 3mgl$ has been added. Consequently, the energy of the system in its balancing position is represented by $P(0) + P_{off}$. Such a reference value for the potential energy ensures the total energy $E(q, \dot{q})$ to remain nonnegative as time elapses.

The total energy of the inverted pendulum considering (3.23) is:

$$E(q, \dot{q}) = K(q, \dot{q}) + P(q) + P_{off}$$

$$= \frac{1}{2} \begin{bmatrix} \dot{x} \\ \dot{\theta} \end{bmatrix}^T \mathbf{M}(\theta) \begin{bmatrix} \dot{x} \\ \dot{\theta} \end{bmatrix} + mgl(cos\theta - 1) + 3mgl \qquad (4.1)$$

In an unforced system, to equilibrium points it corresponds a zero derivative of $P(q)$:

$$\frac{\partial P(q)}{\partial q} = 0 \Rightarrow -mgl\sin(\theta) = 0.$$

Those equilibria result to be $[q, \dot{q}]^T = [i\pi, 0]$, $i \in \mathbb{Z}$. The second derivative of $P(q)$ instead is negative for $q = 0$ and positive for $q = \pi$. Origin corresponds then to a local maximum of the potential energy (unstable) while $q = \pi$ is a minimum (stable).

As said, potential energy in the reference point is $P(0) + P_{off} = 0 + 3mgl$ while in the downright position, at a distance of $2l$ from the reference, it is equal to $3mgl + mgl(\cos\theta - 1) = mgl$. So, it is $P(q) \in [mgl, 3mgl]$. The offset P_{off} has been chosen big enough (but cautiously) to ensure a positive total energy and to do not introduce substantial modifications in the system.

As respects initial kinetic energy, it is proportional to the squared value of the velocity and it assumes its minimum value when velocity is zero. The potential energy of the inverted pendulum is defined [7] as

$$P(q) = mgl(cos\theta - 1)$$

and its derivative is related with the $G(q)$ as

$$\mathbf{G}(q) = \frac{\partial P}{\partial q} \tag{4.2}$$

From equations (3.22)-(3.26) and (3.28)-(4.2) it is obtained the rate of the energy change of system

$$
\begin{aligned}
\dot{E} &= \dot{q}^T \mathbf{M}(q)\ddot{q} + \frac{1}{2}\dot{q}^T \dot{\mathbf{M}}(q)\dot{q} + \dot{q}^T G(q) \\
&= \dot{q}^T \left(-\mathbf{C}(q,\dot{q})\dot{q} - \mathbf{D}\dot{q} - G(q) + \tau + \frac{1}{2}\dot{\mathbf{M}}(q)\dot{q} \right) + \dot{q}^T G(q) \\
&= \dot{q}^T \frac{2}{2} \left(-\mathbf{C}(q,\dot{q})\dot{q} - \mathbf{D}\dot{q} + \frac{1}{2}\dot{\mathbf{M}}(q)\dot{q} \right) + \dot{q}^T \tau \\
&= \frac{1}{2}\dot{q}^T \left(\dot{\mathbf{M}}(q) - 2\mathbf{C}(q,\dot{q}) \right)\dot{q} + \dot{q}^T \tau - \dot{q}^T \mathbf{D}\dot{q} \\
&= \dot{q}^T \tau - \dot{q}^T \mathbf{D}\dot{q} \\
&= \dot{q}^T \begin{bmatrix} u \\ 0 \end{bmatrix} - \dot{q}^T \begin{bmatrix} \gamma & 0 \\ 0 & \gamma_r \end{bmatrix} \dot{q} \\
&= \dot{x}u - \dot{x}^2\gamma - \dot{\theta}^2\gamma_r
\end{aligned}
\tag{4.3}
$$

Homoclinic Orbit

Consider the non linear system

$$\dot{x} = f(x) \tag{4.4}$$

with $f : D \to R^n$ and $\bar{x}$ an equilibrium point of (4.4); that is $f(\bar{x}) = 0$.

The n-dimensional solution can be presented, for a more clear and nice representation, with a set of oriented curves along all points of a 2-dimensional Cartesian plane $(\theta, \dot{\theta})$, called as *phase plane*. This set of curves is called the *phase portrait* of the system (4.4).

The oriented curves traced by the solutions of system of differential equations, are called *orbits* or *trajectories* and demonstrate how the solutions of the system change. A solution of the system (4.4) is an equilibrium point (x_1, x_2). A saddle point is a type of equilibrium point which does not correspond to a local extremum on both axis of a system phase portrait.

In the two dimensional phase plane, a typical periodic (closed) orbit of non linear mechanics is the *limit cycle*. Inside a limit cycle there is at least one trajectory that spirals as time elapses. When the neighbouring orbits of a limit cycle go asymptotically towards to it as $t \to +\infty$, the limit cycle is characterized as stable as it is shown in figure 4.1(a). In contrast, if the trajectories start from neighbouring points of a limit cycle and tend away from it as $t \to \infty$, then the limit cycle is unstable [12].
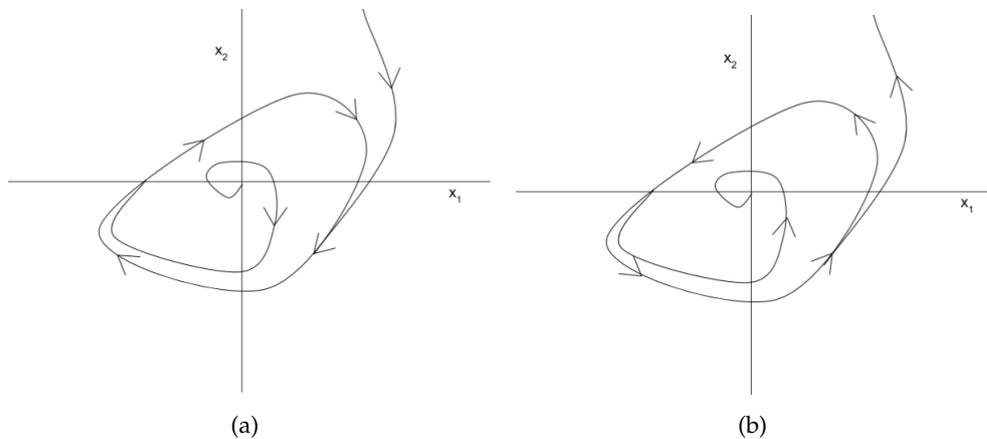
Figure 4.1: (a) stable and (b) unstable limit cycle

A *homoclinic orbit* is a special case of a single orbit which leaves a saddle point in one direction and returns to the same saddle point from another direction as it is shown in figure 4.2(b). Such a homoclinic orbit can express the behaviour of a

dynamical system such as a frictionless pendulum that oscillates around a stable equilibrium point (figure 4.2(a)). For several constant values of E, equation (4.1) describes a possible orbit in the phase plane.
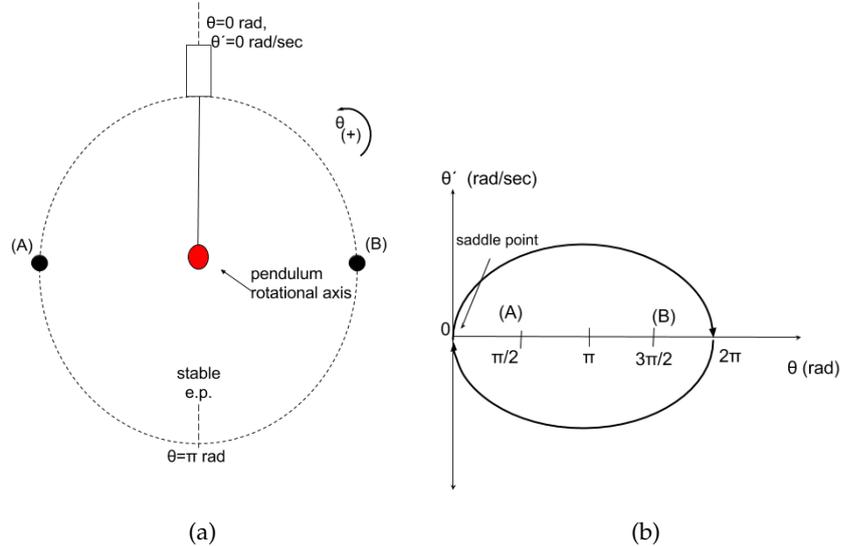
Figure 4.2: Homoclinic orbit example

In the present study, the behavior of the cart pendulum system can be represented in a phase plane, where variables are angular position (θ) and angular velocity ($\dot{\theta}$).

At any instant of time, the system is characterized by a certain pair ($q, \dot{q}$) due to its motion. This variable pair traces out a phase plane orbit which corresponds to a specific total energy E according to (4.1). Different initial conditions for the system give different values of total energy E, hence different orbits. The behavior of the system can be shown through its phase portrait which can be used to obtain the various values of the total energy E of the system. Due to the potential energy offset (P_{off}), the total energy will now converge to $3mgl$ when q and $\dot{q}$ converge to zero as it is referred in section 4.2.

Substituting matrices from (3.23) in equation (4.1) and considering $\dot{x} = 0$ and $E(q, \dot{q}) = 3mgl$, for the case of an upright stabilized inverted pendulum it is ob-

tained

$$K(q,\dot{q}) + P(q) + P_{off} = \frac{1}{2}\dot{\theta}^2 ml^2 + mgl(cos\theta - 1) + P_{off} \Rightarrow$$

$$\underbrace{K(q,\dot{q}) + P(q)}_{=0} + 3mgl = \frac{1}{2}\dot{\theta}^2 ml^2 + mgl(cos\theta - 1) + 3mgl \Rightarrow$$

$$\frac{1}{2}\dot{\theta}^2 ml^2 = -mgl(cos\theta - 1) \tag{4.5}$$

which expresses the homoclinic orbit [10]. Also, when $\theta = 0$ (then $\dot{\theta} = 0$), the pendulum has reached an equilibrium point. Generally, when the pendulum is in the region $\theta \in [0, 2\pi]$, the system (3.22) has two sets of equilibrium points: $(x, \theta, \dot{x}, \dot{\theta}) = (\alpha, 0, 0, 0)$ for the unstable equilibrium points, $(x, \theta, \dot{x}, \dot{\theta}) = (\alpha, \pi, 0, 0)$ for the stable equilibrium points, where (α) can be any possible value of the cart displacement x.

If the system can be brought to the homoclinic orbit then the task of swinging up the pendulum has been solved since the pendulum, eventually, will approach an unstable equilibrium point if it follows the homoclinic orbit. Finally, the swing up control will be switched to a linear controller which will ensure (local) asymptotic stability for this equilibrium point and will stabilize the pendulum in the upright vertical position as described in section 4.4. Moreover, convergence of the system in the homoclinic orbit ensures that the trajectory of the inverted pendulum will enter the operation range of this linear controller.

Consider the subsystem pendulum: neglecting the friction, the system is conservative. Energy remains constant and its derivative is zero. Adding friction, energy decreases, because of dissipation, with derivative $\frac{\partial E}{\partial t} \leq 0$ and the trajectory tends to the stable equilibrium point. The study of the derivative of $E(q, \dot{q})$ along the trajectory of the system provides informations about the stability of the equilibrium point. Certain mathematical function could be used in the study of stability of equilibrium points rather than energy [12] . Changes over time on such an energy-like function (V), introduced by Lyapunov, might reveal conclusions about the trajectories of a system without finding the trajectories.

Lyapunov Stability

Consider a function $V : R^n \rightarrow R$ that satisfy some conditions on V and $\dot{V}$, than trajectory of the system satisfies some property. If such a function V exists, it is called *Lyapunov function*. Depending on the system's equations, there will be a different V for each different system.

Theorem 4.3.1 (Lyapunov's stability) *Let $x = 0$ be an equilibrium point for the system (4.4) and $D \subset R^n$ be a domain containing $x = 0$. Let $V : D \to R$ be a continuously differentiable function such that*

$$V(0) = 0 \quad and \quad V(x) > 0 \quad in \quad D - \{0\}$$
$$\dot{V} \leq 0 \quad in \quad D$$

Then, $x = 0$ is stable. Moreover, if

$$\dot{V} < 0 \quad in \quad D - \{0\}$$

then $x = 0$ is asymptotically stable [12].

The aim to design a Lyapunov function based on the mechanical energy is discussed. The proposed candidate function is expressed as the sum of squares of total energy, position and velocity of the cart. The purpose is to have all the terms of $V(q, \dot{q})$ equal to zero in the upright position:

$$V = \frac{K_E}{2} \left(E - P_{off} \right)^2 + \frac{K_v}{2} \dot{x}^2 + \frac{K_x}{2} x^2 \tag{4.6}$$

where gains K_E, K_v, K_x are strictly positive constants. Lyapunov's stability theorem (4.3.1) requires the candidate function (4.6) to be positive definite but from the expression of energy (4.1) it is possible to get $E - P_{off} = 0$ by combination of θ and $\dot{\theta}$ values other than zero. Therefore, (4.6) is not a Lyapunov function . Failing to design a Lyapunov function does not preclude alternative approaches: conditions in Lyapunov's stability theorem are only sufficient.

Theorem 4.3.2 (LaSalle's theorem) *Let $\Omega \subset D$ be a compact set that is positively invariant with respect to (4.4). Let $V : D \to R$ be a continuously differentiable function such that $\dot{V} \leq 0$ in Ω. Let $\mathcal{E}$ be the set of all points in Ω where $\dot{V} = 0$. Let M be the largest invariant set in $\mathcal{E}$. Then every solution starting in Ω approaches M as $t \to \infty$ [12].*

LaSalle's theorem allows us to use function (4.6) also if it is not positive definite; there are conditions only on the derivative of $V(q, \dot{q})$. It extends Lyapunov's theorem (4.3.1) and can be used when, instead of an isolated equilibrium point, the system has an equilibrium set [12]. In return, the construction of the set Ω is required. When $V(q, \dot{q})$ is radially unbounded (as function (4.6)), it is possible to define a set $\Omega_c = \{(q, \dot{q}) \in R^n | V(q, \dot{q}) \leq c\}$ bounded for all the values of c. The set Ω_c represents an estimation for the region of attraction to the equilibrium set [12].Using the LaSalle's theorem principle, a control law will be designed to bring the pendulum to the invariant set M, starting from a region of attraction.

As it was referred in section 4.2.1, in this study the inverted pendulum has a set of equilibrium points instead of a unique equilibrium point. Furthermore, the

non linear energy control that performs the swing up motion of the pendulum will eventually switch to a linear control when the pendulum arrives in a narrow region around the upright vertical position such that to stabilize it. The linear controller K_1 designed in [4] is used for the stabilization of the pendulum in the upright vertical position. Experimentally it has been found that the controller K_1 is able to stabilize the pendulum from an initial angle $\theta \in (-0.262, +0.262)[rad]$ (or $\theta \in (-15^o, +15^o)$). Therefore, by switching from the non linear energy control to the linear control for a pendulum displacement $\theta \in [-0.175, +0.175][rad]$ (or $\theta \in [-10^o, +10^o]$) it is ensured that finally the linear controller will execute the control task.

Control Law Formulation

Since frictions ($F_f = F_c + \gamma \dot{x}$) acting during the linear motion of the cart will be compensated by the microcontroller (section 2.2), control law u will be designed considering $u = F_M - F_f$. Therefore, the system dynamics (3.20) is transformed to

$$(M+m)\ddot{x} - ml\dot{\theta}^2 \sin\theta + ml\ddot{\theta}\cos\theta = u$$
$$ml^2\ddot{\theta} - mgl\sin\theta + ml\cos\theta\ddot{x} = \gamma_r \dot{\theta} \qquad (4.7)$$

It follows that state equations for $\ddot{x}$ (3.32) and $\ddot{\theta}$ (3.33) become:

$$\ddot{x} = \frac{m\sin\theta(l\dot{\theta}^2 - g\cos\theta) + \frac{\gamma_r\cos\theta\dot{\theta}}{l} + u}{M + m\sin^2\theta} \qquad (4.8)$$

$$\ddot{\theta} = \frac{-m^2l^2\sin\theta\cos\theta\dot{\theta}^2 - (M+m)\gamma_r\dot{\theta} + (M+m)gml\sin\theta - ml\cos\theta u}{ml^2(M + m\sin^2\theta)} \qquad (4.9)$$

where terms with $\gamma\dot{x}$ disappeared.

Expression (4.3) for $\dot{E}$ is also affected by this change:

$$\dot{E} = \dot{x}u - \dot{\theta}^2\gamma_r \qquad (4.10)$$

The derivative of $V(q, \dot{q})$, using the equation (4.10), is

$$\begin{aligned}
\dot{V} &= K_E(E - P_{off})\dot{E} + K_v\dot{x}\ddot{x} + K_x x\dot{x} \\
&= K_E(E - P_{off})(\dot{x}u - \dot{\theta}^2\gamma_r) + K_v\dot{x}\ddot{x} + K_x x\dot{x} \\
&= \dot{x}\left[K_E(E - P_{off})u + K_v\ddot{x} + K_x x\right] - \dot{\theta}^2\gamma_r K_E(E - P_{off}) \qquad (4.11)
\end{aligned}$$

For simplicity, equation (4.8) is redefined as

$$\frac{m\sin\theta(l\dot{\theta}^2 - g\cos\theta) + \frac{\gamma_r\cos\theta\dot{\theta}}{l} + u}{M + m\sin^2\theta} = \frac{\alpha(\theta, \dot{\theta}) + u}{\beta(\theta)} \qquad (4.12)$$

and substituting (4.12) into (4.11), it is obtained

$$\dot{V} = \dot{x}\left[K_E(E - P_{off})u + K_v\left(\frac{\alpha(\theta,\dot{\theta}) + u}{\beta(\theta)}\right) + K_x x\right] - \dot{\theta}^2\gamma_r K_E(E - P_{off}) \qquad (4.13)$$

A large level of the system potential energy in the unstable equilibrium point en-
sures the cart pendulum total energy E to be always positive, as it is referred in
section 4.2. Thus, term $-\dot{\theta}^2\gamma_r K_E E$ in equation (4.13) is always negative and it is not
considered in the design of the control law u. Consequently, the following control
law is proposed based on (4.13)

$$K_E(E - P_{off})u + K_v\frac{\alpha(\theta,\dot{\theta}) + u}{\beta(\theta)} + K_x x = -K_\delta \dot{x} \Rightarrow$$

$$u\left(K_E(E - P_{off}) + \frac{K_v}{\beta(\theta)}\right) + K_v\frac{\alpha(\theta,\dot{\theta})}{\beta(\theta)} + K_x x = -K_\delta \dot{x} \qquad (4.14)$$

that gives

$$u = \frac{\beta(\theta)(-K_\delta \dot{x} - K_x x) - K_v\alpha(\theta,\dot{\theta})}{\beta(\theta)K_E(E - P_{off}) + K_v}. \qquad (4.15)$$

Control law u is defined if singularities in (4.14) are avoided. Thus, seen (4.12), it
exists:

$$K_E(E - P_{off}) + \frac{K_v}{\beta(\theta)} \neq 0 \Rightarrow$$

$$\frac{K_v}{K_E} \neq -(E - P_{off})(M + m\sin^2\theta) \qquad (4.16)$$

Considering the total energy of system (4.1), term $(E - P_{off})$ is not smaller than
$-2mgl$:

$$E - P_{off} \geq -2mgl \qquad (4.17)$$

From (4.16) and (4.17), the following constrain is achieved

$$\frac{K_v}{K_E} > 2mgl \, max_\theta\{M + m\sin^2\theta\} \Rightarrow$$

$$\frac{K_v}{K_E} > 2mgl(M + m) \simeq 5.11 \qquad (4.18)$$

The ratio of K_v to K_E will be provided according to inequality (4.18). Substituting
(4.14) in (4.13) it is obtained

$$\dot{V} = -K_\delta \dot{x}^2 - \dot{\theta}^2\gamma_r K_E(E - P_{off}) \qquad (4.19)$$

where $K_\delta > 0$ to ensure that $\dot{V}(q, \dot{q})$ is negative semi definite as required in the *LaSalle's invariance principle*. Control gains in control law (4.15) have been chosen according to bibliography as well as simulation tests such that to give a high pendulum oscillation as much close to its unstable equilibrium point. They are determined as:

$$K_x = 14, \quad K_\delta = 2, \quad K_v = 5.5, \quad K_E = 1 \tag{4.20}$$

Equation (4.5) reveals us the energetic level where we want the system to be. The relative phase portrait plot of (4.5) is shown in figure 4.3.
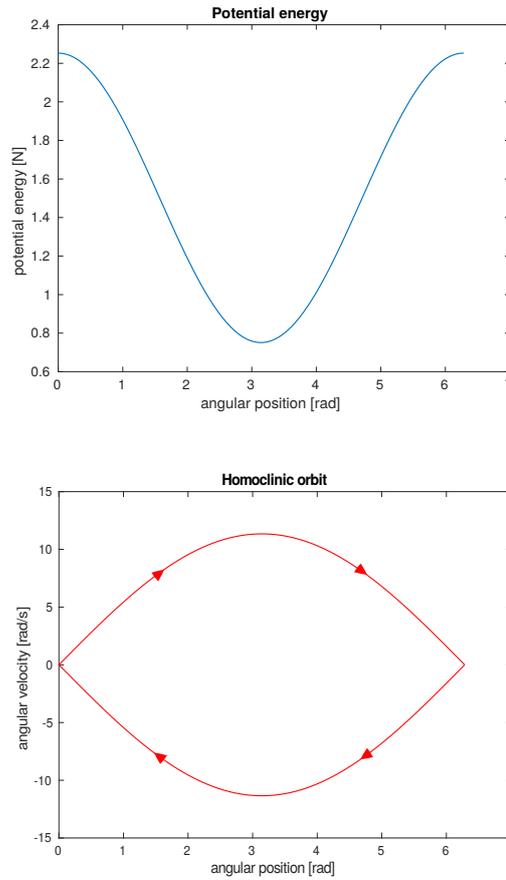
Figure 4.3: System's potential energy and homoclinic orbit reference.

Its shape varies with the potential energy shape. To the maxima of potential energy (P), correspond the unstable points $0[rad]$ and $6.28[rad]$, to its minimum the stable point $3.14[rad]$. Homoclinic orbit separates the trajectories circling the stable point from those circling the two unstable points [19].

The nonlinear strategy here presented is not able to reach that level. It will be showed instead that, by means of the swing up, system will converge as close as possible to that orbit.
Simulations in figure 4.4 for the closed loop system using the control law (4.15) revealed that the pendulum can not reach the desired range where the linear controller works. A reason could be the rotational viscous friction in the pendulum,
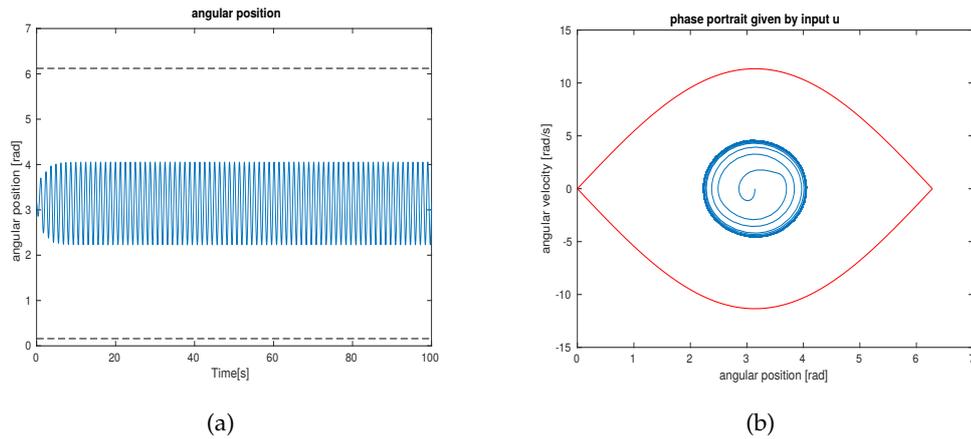
Figure 4.4: Angular position and phase portrait simulation using control law (4.15).

since these non conservatives forces usually create difficulties in modeling and controlling a system. The underactuated system can not directly overcome it. To verify such an assumption a simulation removing the rotational friction from the system ($\gamma_r = 0$) has been run. Figure 4.5 shows that, without the rotational friction, control law u is able to bring the pendulum in a vicinity of the upright position, while the orbit goes close to the homoclinic one.

(a)   (b)
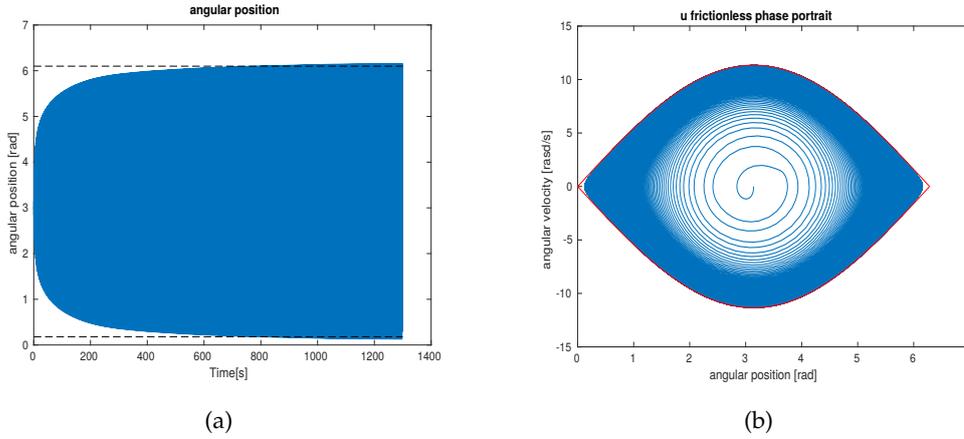
Figure 4.5: Angular position and phase portrait simulation using control law (4.15) while rotational friction has been removed.

Being the friction removed, can be seen that quite long time is required to reach the result. Trying to tune differently the gains could help to reach earlier the same result.

Formulation of the additional control term v

Taking into account results from figure 4.4 and 4.5, it can be said that the dissipation term $\gamma_r\dot{\theta}$ can be considered as an uncertainty, that affects the control of the system. Thus, an additional feedback control term v should be designed in order to compensate the effect of γ_r in the closed loop equation of the pendulum (4.9) and stabilize the actual system from this uncertainty.

$$\ddot{\theta}_{new} = \frac{-m^2l^2 sin\theta cos\theta \dot{\theta}^2 - (M+m)\gamma_r\dot{\theta} + (M+m)gmlsin\theta - mlcos\theta(u_{tot})}{ml^2(M+msin^2\theta)} \quad (4.21)$$

where $u_{tot} = u + v$ is the overall controller that eventually will stabilize the pendulum in the upright vertical position.

According to [9], the additional term v is designed based on the expectation that equation (4.21) (that presents rotational friction term and correction term v) coincide with equation (3.33) for the case without friction ($\gamma_r = 0$) and relative

compensation, as it is shown below.

$$\ddot{\theta}|_{(\gamma_r=0)} = \ddot{\theta}_{new} \Rightarrow$$
$$\frac{-m^2l^2sin\theta cos\theta\dot{\theta}^2 + (M+m)gmlsin\theta - mlcos\theta u}{ml^2(M+msin^2\theta)} =$$
$$\frac{-m^2l^2sin\theta cos\theta\dot{\theta}^2 - (M+m)\gamma_r\dot{\theta} + (M+m)gmlsin\theta - mlcos\theta(u+v)}{ml^2(M+msin^2\theta)}$$

Removing terms present in both sides of the equality, it remains:

$$\frac{mlcos\theta}{ml^2(M+msin^2\theta)}v = \frac{-(M+m)\gamma_r\dot{\theta}}{ml^2(M+msin^2\theta)} \Rightarrow$$
$$v = \frac{\left(-(M+m)\gamma_r\dot{\theta}\right)\left(ml^2(M+msin^2\theta)\right)}{\left(ml^2(M+msin^2\theta)\right)(mlcos\theta)} \Rightarrow$$
$$v = -\frac{M+m}{mlcos\theta}\gamma_r\dot{\theta} \tag{4.22}$$

As a consequence, it is formulated the following control law based on a desired total energy (4.5) and a desired closed loop structure (4.21). The inverted pendulum, considering also the non conservative forces, is swung up by this control input that ensures also convergence to the operational range of the linear controller.

Setting $u = u_{tot} - v$ in equation (4.13) it is obtained:

$$\dot{V} = \dot{x}\left[K_E(u_{tot}-v)E + K_v\left(\frac{\alpha(\theta,\dot{\theta})+(u_{tot}-v)}{\beta(\theta)}\right) + K_x x\right] - \dot{\theta}^2\gamma_r K_E E$$

where

$$K_E(u_{tot}-v)E + K_v\left(\frac{\alpha(\theta,\dot{\theta})+(u_{tot}-v)}{\beta(\theta)}\right) + K_x x = -K_\delta\dot{x} \Rightarrow \tag{4.23}$$

$$u_{tot}\left(K_E E + \frac{K_v}{\beta(\theta)}\right) - v\left(K_E E + \frac{K_v}{\beta(\theta)}\right) + \frac{K_v\alpha(\theta,\dot{\theta})}{\beta(\theta)} + K_x x = -K_\delta\dot{x} \Rightarrow$$

$$u_{tot}\left(K_E E + \frac{K_v}{\beta(\theta)}\right) = -K_\delta\dot{x} + v\left(K_E E + \frac{K_v}{\beta(\theta)}\right) - \frac{K_v\alpha(\theta,\dot{\theta})}{\beta(\theta)} - K_x x \Rightarrow$$

$$u_{tot} = \frac{(-K_\delta\dot{x} - K_x x)\beta(\theta) - K_v\alpha(\theta,\dot{\theta})}{\beta(\theta)K_E E + K_v} + v \tag{4.24}$$

with v as defined in (4.22)

From equations (4.23), (4.13) the derivative of the function V is obtained, which should be negative semi definite as it is required in the *LaSalle's invariance principle*:

$$\dot{V} = -K_\delta\dot{x}^2 - \dot{\theta}^2\gamma_r K_E E \tag{4.25}$$

For $K_\delta > 0$, it gives $\dot{V} \le 0$, thus the control law (4.24) can be used for the swinging of the pendulum.

Additional controller v in equation (4.22) has a singularity for values of θ close to $(\frac{\pi}{2} + k\pi)[rad]$, when $\cos\theta$ is very close to zero. As a consequence, while pendulum rod were close to the horizontal positions, DC motor would be required to release a very high torque. This eventuality can be avoided introducing a limitation to the value assumed by the function v. During the entire swing up, additional controller (4.22) is then compared with the function

$$v_{max} = -\frac{M+m}{ml\cos(1.435)}\gamma_r\dot{\theta}.$$

where the argument of $\cos(\theta)$ in (4.22) has been substituted with $1.435[rad]$ (or 82°). For a range of θ about $(\frac{\pi}{2} + k\pi)[rad]$, v becomes too large: it is imposed to the additional term to switch to the value $\texttt{sign}(\frac{v}{v_{max}})$ when $v > v_{max}$. Under this condition, singularity is avoided and the motor is not overloaded.
A saturation function, as said in (2.2), is already present in the `Utility.cpp` library; it is reported in Listing 4.1.

Listing 4.1: Saturation function.

```
17  float sat(float x, float eps) {
18      if (abs(x) > 1) {
19          return sign(x);
20      }
21      else {
22          return x*(1/eps);
23      }
24  }
```

With the purpose of writing a clean code, this saturation function has been used to implement the definitive controller in the Arduino code as well as the Matlab code has been built following the same structure. So, additional controller v from equation (4.22) becomes:

$$v = \texttt{sat}\left(\frac{v}{v_{max}}, \frac{1}{v_{max}}\right) \tag{4.26}$$

From a Matlab simulation plot, v is represented as in figure 4.6. It is easy to see that it assumes the highest values when the pendulum is close to the horizontal positions; singularity is avoided switching v to ± 1.
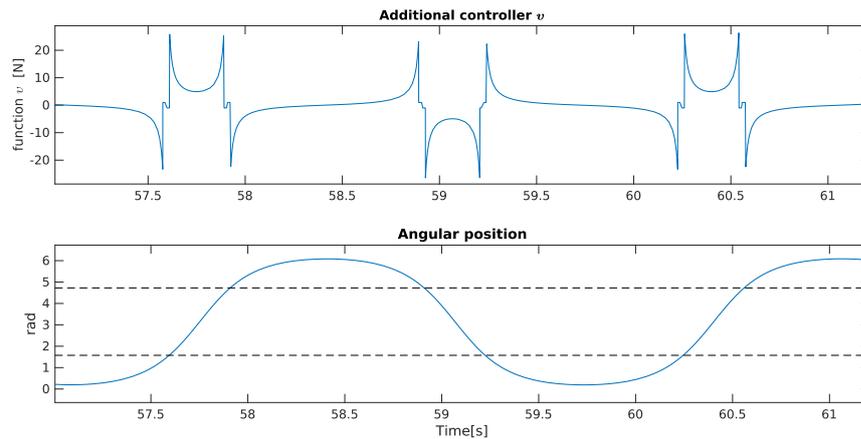
Figure 4.6: Additional controller v from Matlab simulation.

Introducing (4.26) in the equation (4.24), it is attained:

$$u_{tot} = \underbrace{\frac{(-K_\delta \dot{x} - K_x x)\beta(\theta) - K_v \alpha(\theta, \dot{\theta})}{\beta(\theta) K_E E + K_v}}_{u} + \underbrace{\text{sat}\left(\frac{v}{v_{max}}, \frac{1}{v_{max}}\right)}_{v} \qquad (4.27)$$

Simulation in figure 4.7(a) using controller (4.27) shows that the system is able to bring the pendulum close to the upright position, in a region where the linear controller performs well.

(a)

(b)
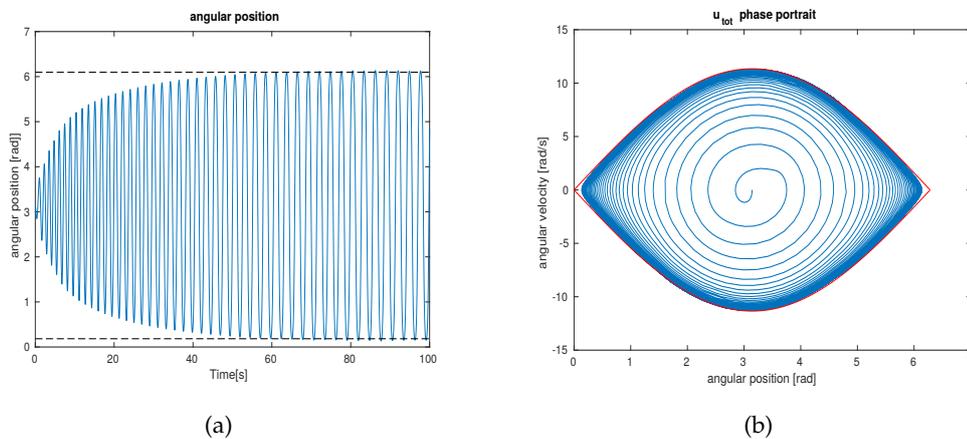
Figure 4.7: Angular position and phase portrait simulation using control law (4.27).

Running the same simulation for a very long time, it is possible to see the effect of the control law (4.27) while there is no switch to the linear controller. Figure 4.8

shows the system converged to a set of orbit representing the invariant set M, as stated in LaSalle's theorem 4.3.
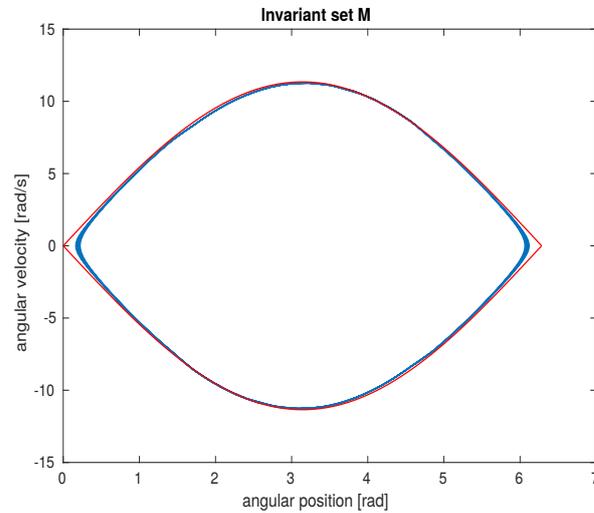
Figure 4.8: Phase portrait showing the invariant set M (in blue) where the system converges during the swing up. Plotting time range is $3000 \div 4000$[s].

An outlook of the complete scenario is given in figure 4.9, where the homoclinic reference, the invariant set M and the possible Ω sets are depicted.
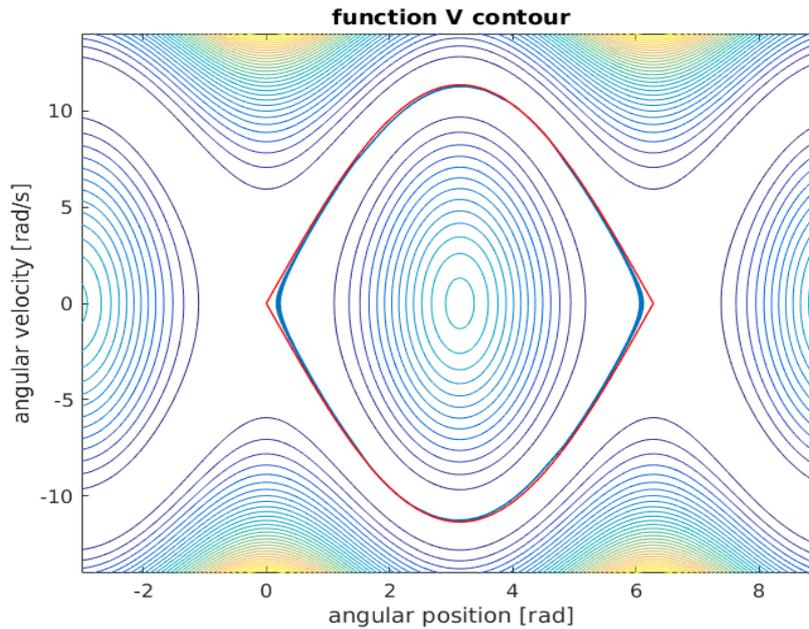
Figure 4.9: Phase portrait showing various Ω sets inside and outside the stable set M.

In figure 4.9, the Ω sets surrounded by set M are good enough estimations of the region of attraction. Outside the M set and the homoclinic orbit, sets Ω become open. LaSalle's theorem (4.3) refers to those Ω sets that are compact. Nothing can be said if they are not.

Simulation

The final desired behaviour of the controlled inverted pendulum can be distinguished in two parts. Initially, the system with the applied control law (4.27) swings the pendulum from a downright position to an upright position. Afterwards, when the pendulum displacement is close to an unstable equilibrium point $(-0.175[rad] < \theta < 0.175[rad])$ the applied swing up energy control switches to a linear control that stabilizes the pendulum upright vertically. Matlab ode23 function has been used to simulate the behavior of the non linear system.

Totally, simulation was performed for initial conditions $(x, \theta, \dot{x}, \dot{\theta}) = (0.25[m], \pi[rad], 0, 0)$. The used controller gains are:

- linear controller: $K_1 = [-30.6130 - 121.4494 - 22.5738 - 17.1256]$ as it is presented in the Appendix A

- swing up energy controller: $K_x = 14, \quad K_\delta = 2, \quad K_v = 5.5, \quad K_E = 1$

(a)

(b)
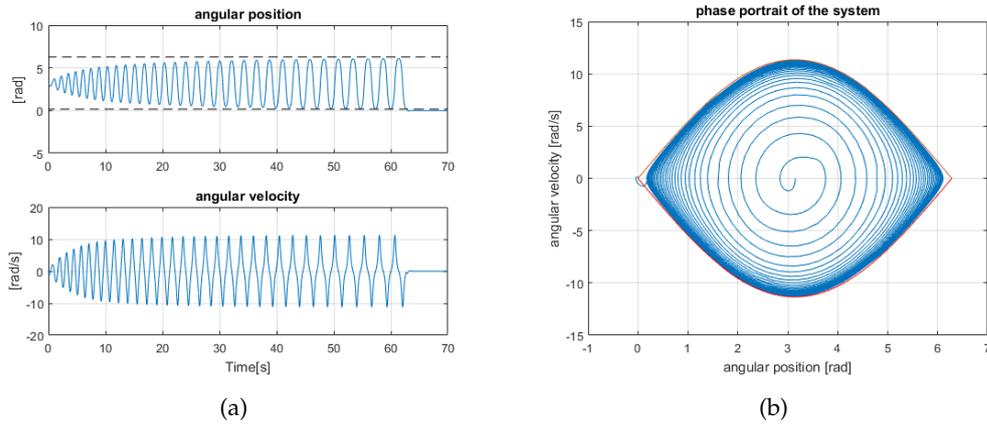
Figure 4.10: System response. The dashed lines in figure 4.10(a) defines in which angles the switching to the linear controller is executed. The homoclinic orbit is presented with red color in figure 4.10(b)

Figure 4.10 demonstrates the simulated response of the system. The angular position and velocity of the pendulum are increasing regularly until the time of 63[s] where the pendulum reaches an angle $\theta = 0.175[rad]$ as it is shown in figure 4.10(a). At this point the swing up control switches to the linear control such that the pendulum to be stabilized upright vertically. Thus, after 63[s] the pendulum displacement and velocity are almost equal to 0. Figure 4.10(b) shows the orbits followed by the pendulum. The pendulum arrives very close to the reference of homoclinic orbit (red orbit) but since it is not able to reach it, the control switches to a linear one that will stabilize the pendulum.It should be referred that the M invariant set shown in plot 4.8 contains pendulum angles which are inside the operational range of the linear controller. In this way it is guaranteed that eventually the swing up control switches to the linear one.

As final step in the analysis performed in this chapter, some considerations about the energy are given. In figure 4.11 the level of the system energy (4.1) is presented: during the swing up, the energy starts from the value $mgl(= 0.751)[J]$ and it reaches the value $3mgl(= 2.253)[J]$ before the switching in $t = 63[s]$. Initial and final values for the total energy are those of the potential energy, as in figure 4.3. Energy remains every time positive during the simulation, as required in section 4.2.
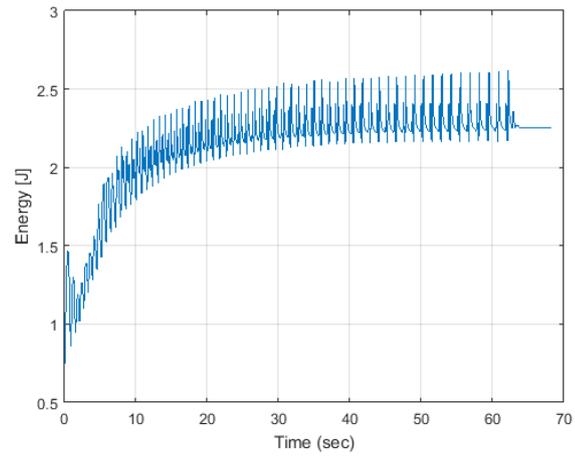
Figure 4.11: Simulated energy of the system

Chapter 5

Laboratory implementation

Introduction

This chapter presents the implementation and tuning process of the swing up controller in the inverted pendulum. The control law (4.27), as well as the energy controller (4.20) are implemented in the physical inverted pendulum set up shown in figure 3.5. Simulation results which are presented in sections 4.3.1 and 4.4, were used as guidelines. Due to implementation issues, the control law (4.27) should be adjusted accordingly in order to achieve:

- a swing up motion that gives to the pendulum a proper velocity $\dot{\theta}$

- a steady switching from the swing up controller to the linear controller which eventually stabilize the pendulum upright

Initially, a scaling factor η is introduced in the applied control law to achieve the first objective. The value of this coefficient is defined with a tuning process which consists of two steps as it is presented in section 5.2. Afterwards, a second scaling factor η_2 is also applied in the control law in order to reach the second objective.

It is convenient to recall the designed control laws presented in section 4.3.1 since they were used during the tuning procedure.
Control law (4.15):

$$u = \frac{\beta(\theta)(-K_\delta \dot{x} - K_x x) - K_v \alpha(\theta, \dot{\theta})}{\beta(\theta) K_E (E - P_{off}) + K_v}$$

The pendulum oscillates within the range of $2.22[rad] < \theta < 4.05[rad]$.

Control law (4.27):

$$u_{tot} = \underbrace{\frac{(-K_\delta \dot{x} - K_x x)\beta(\theta) - K_v \alpha(\theta, \dot{\theta})}{\beta(\theta)K_E E + K_v}}_{u} + \underbrace{\text{sat}\left(\frac{v}{v_{max}}, \frac{1}{v_{max}}\right)}_{v}$$

The pendulum swinging up approaching the upright vertical position where a linear controller acts.

1st Control Adjustment: Swing Up Tuning

For an initial cart displacement of $x_{init} = 0,25[m]$, as well as a pendulum displacement of $\theta_{init} = \pi[rad]$, the response of the real system was obtained using the control law (4.27)). Figure 5.1 demonstrates that with the usage of this control law the pendulum swings up from its initial angle $\theta_{init} = \pi[rad]$ but it is not able to be stabilized from the linear controller, with gains K_1, since the pendulum angle does not remain steady in an angle of 0 or $6.28[rad]$ eventually. The linear controller K_1 operates in the angle range of $-0.175[rad] < \theta < 0.175[rad]$.

(a)   (b)
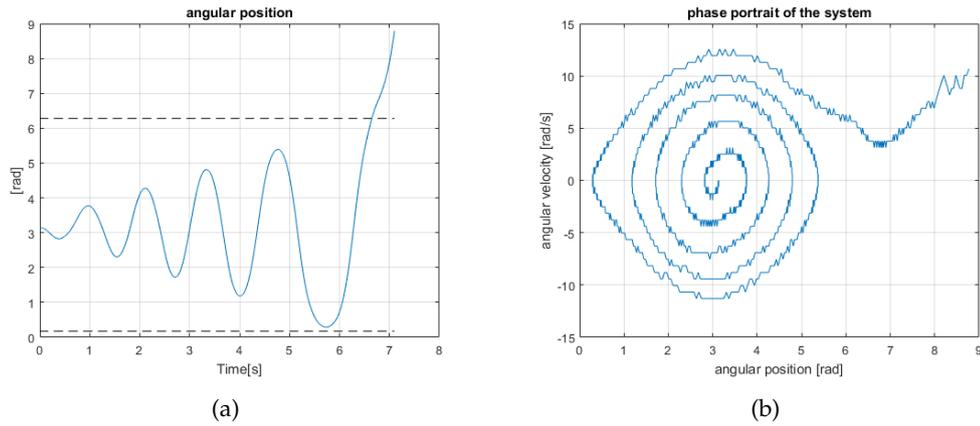
Figure 5.1: System response using the control law (4.27)

A reason for this issue could be a large pendulum velocity ($\dot{\theta}$) when the pendulum enters the linear controller operational range. Consequently, the linear controller is not able to stabilize the pendulum upright. Practically, that may mean that the applied force of the motor (F_M) is higher than the one which has been designed and simulated for the energy controller that performs the swing up motion of the inverted pendulum. Due to the fact that simulation results presented in section 4.4 show an acceptable performance with a pendulum stabilized upright, it

can be said that there is an implementation issue or a model uncertainty may exist.

Initially, from the control law (4.27) the additional control input term (v) which compensates the rotational friction of the pendulum ($\gamma_r \dot{\theta}$) is disregarded. Now, the applied control law is the (4.15). In this case, the pendulum reaches the operational range of the linear controller ($-0.175[rad] < \theta < 0.175[rad]$, dashed lines) as it is shown in figure 5.2. Also, the pendulum is stabilized upright vertically. Apparently, this is an undesired behaviour because simulations in subsection 4.3.1 revealed that in such a case the pendulum should not reach the operational range of the linear controller.

(a)   (b)
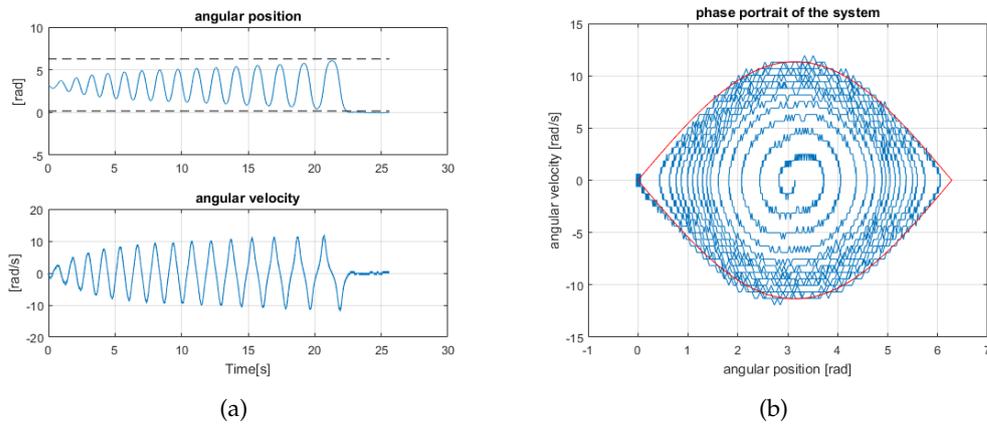
Figure 5.2: System response for the control law (4.15)

In an attempt of following the simulation results, a scaling coefficient η is introduced proportional to the control law (4.27) in order to regulate the applied control input. After that, the applied swing up control law in the real system is defined as:

$$u_{tot} = \eta \left(\underbrace{\frac{(-K_\delta \dot{x} - K_x x)\beta(q) - K_v \alpha(q, \dot{q})}{\beta(q)K_E E + K_v}}_{u} + \underbrace{sat\left(\frac{v}{v_{max}}, \frac{1}{v_{max}}\right)}_{v} \right) \quad (5.1)$$

The response of the system for different values of this coefficient was investigated, according to the following tuning procedure:

- STEP 1 Initially, set a value for the coefficient η and control the system via $u_{tot} = \eta * u$.

- STEP 2 Then, control the system via $u_{tot} = \eta * (u + v)$ and comparison with the corresponding simulation results.

In the next subsection, conclusions from this regulation procedure are presented aiming to results similar with the simulated ones.

Tuning procedure

Imprecise estimated values for the states $\dot{x}$, $\dot{\theta}$ of the system may introduce uncertainties in the system. The swing up motion of an inverted pendulum is a demanding and accurate motion, where small errors may create deviations that results in a failure. With the usage of the scaling coefficient η, a regulation of the control law (5.1) is performed, without modifying the swing up control gains ($K_{\delta}, K_x, K_v, K_E$).

STEP 1

From a starting value of $\eta = 1$, this coefficient was decreased until the real pendulum followed the simulations (figure 4.5(b)) and oscillated ideally close to the region $2.22[rad] < \theta < 4.05[rad]$.

The applied control law is

$$u_{tot} = \eta \underbrace{\left(\frac{(-K_{\delta}\dot{x} - K_x x)\beta(q) - K_v \alpha(q, \dot{q})}{\beta(q)K_E E + K_v} \right)}_{u} \tag{5.2}$$

that corresponds to the theoretical (4.15).

For a value of η=0.279 the pendulum oscillates in the range ($1.77[rad] < \theta < 4.5[rad]$) which is close to the simulation range of $2.22[rad] < \theta < 4.05[rad]$, as it is shown in figures 5.3 and 5.4.

(a)

(b)
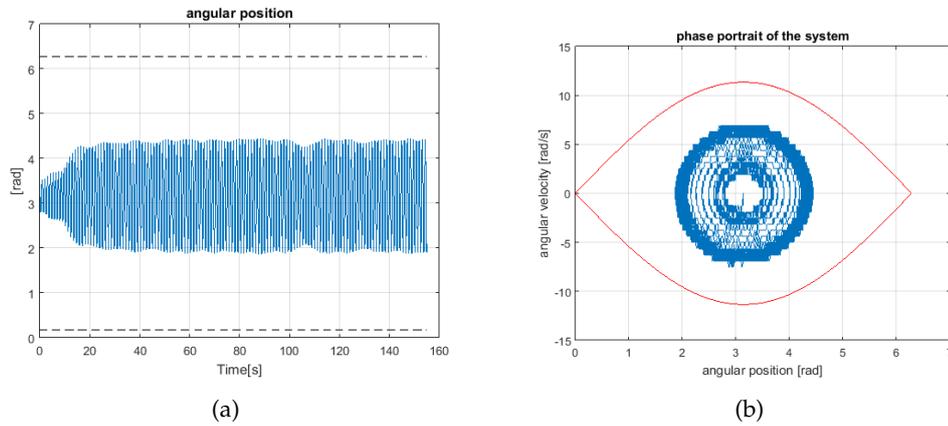
Figure 5.3: System response using the control law (5.2) and coefficient $\eta = 0.279$.
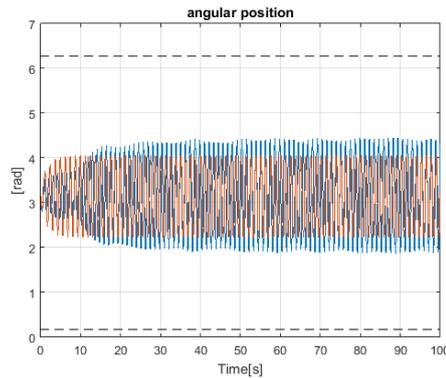
Figure 5.4: Simulated system response (red) and real system response with $\eta = 0.279$ (blue) for the control laws (4.15) and (5.2) respectively.

Now the inverted pendulum has a behaviour that follows the simulations and the related theory referred in section 4.3.1 for the applied control (5.2).

STEP 2

Next step is the implementation of the additional control input term v such that the system to be controlled according to equation (5.1) in order to reach the operational range of the linear controller. For the control law (5.1) and a coefficient $\eta = 0.279$, the response of the system is shown in figure 5.5.

(a)

(b)
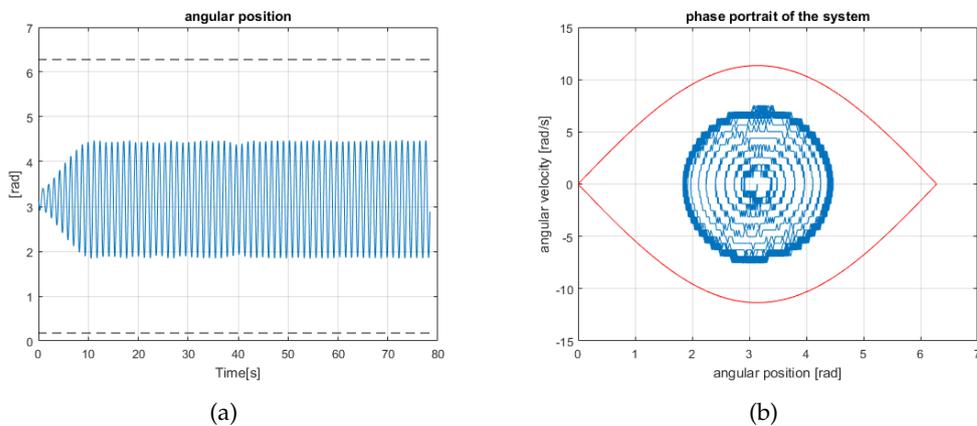
Figure 5.5: System response using the control law (5.1) and coefficient $\eta = 0.279$

Unfortunately the system still does not reach the desired region where the linear control acts (dashed lines) as it is shown from figure 5.5(a). Additional control term v is not able to give any contribution to the swing up procedure if multiplied by the coefficient $\eta = 0.279$. It is concluded that the option of $\eta = 0.279$ can not

be characterized as acceptable, probable because of its low value. For this reason it
is gradually increased, starting this time from the value of 0.279, until the applied
control law (5.1) will place the pendulum in the operational range of the linear
controller with gains K_1 and stabilize it upright vertically. The previous tuning
procedure is repeated. It is now chosen a value $\eta = 1.44$.

STEP 1

As shows figure 5.6, using the control law (5.2) with $\eta = 1.44$, the pendulum does
not arrive to the angular positions $\theta < 0.175[rad]$ or $\theta > 6.125[rad]$. This behaviour
follows what was expected from the simulations.

(a)   (b)
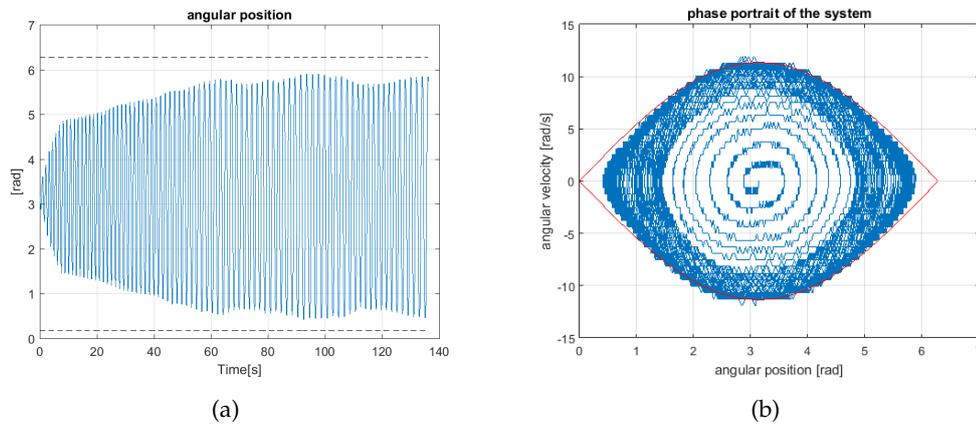
Figure 5.6: System response using the control law (5.2) with a coefficient $\eta = 1.44$.

STEP 2

Afterwards, the control law (5.1) with a coefficient $\eta = 1.44$ was applied in the
system. Figure 5.7 shows the response of the system in this case.

The pendulum reaches the operational range of the linear controller but, ap-
parently, after the switching it is not able to be stabilized upright from the linear
controller. Also, according to figure 5.7(b) the phase portrait of the real pendulum
does not remain close to the reference homoclinic orbit. This fact reveals that the
pendulum is not stabilized upright despite the fact that it reaches the switching
range.

To sum up, for an applied control law (5.2) with coefficient $\eta = 1.44$ the real
inverted pendulum has the same tendency with the simulated one.
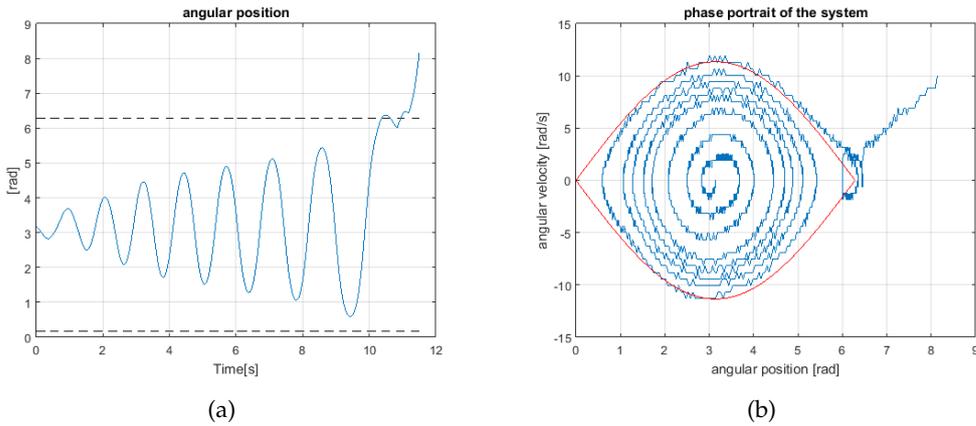
Figure 5.7: System response using the control law (5.1) with coefficient $\eta = 1.44$.

This is demonstrated in figure 5.8 where both the real system angular displacement and the simulated one do not arrive in the switching point to the linear controller (dashed lines). The first objective of a proper swing up motion has been reached.
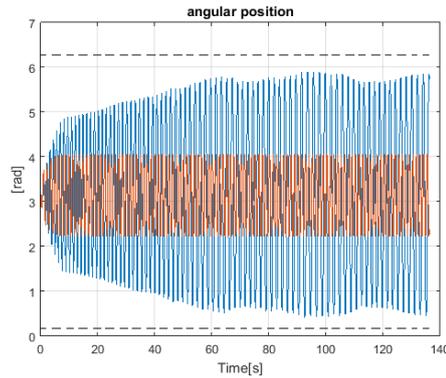
Figure 5.8: Simulated system response (red) and real system response (blue) for a control law (5.2) and a used coefficient $\eta = 1.44$ for the applied control in the real system.

On the other hand, a smooth control switch to the linear controller has not been reached yet as it is shown in figure 5.7. Thus, the form of the applied control law (5.1) should be modified as an attempt to better results.

2nd Control Adjustment: Stable Switching Tuning

In this part is presented how it is faced the problem of the failed linear control after the control switching from the swing up energy control. According to the referred theory in section 4.3.1, the applied control law in the physical inverted pendulum should have the form of (5.1) that corresponds to the theoretical (4.27). Initially, the form of the applied law (5.1) has been modified to

$$u_{tot} = \eta \left(\underbrace{\frac{(-K_\delta \dot{x} - K_x x)\beta(q) - K_v \alpha(q, \dot{q})}{\beta(q) K_E E + K_v}}_{u} \right) + \underbrace{sat \left(\frac{v}{v_{max}}, \frac{1}{v_{max}} \right)}_{v} \qquad (5.3)$$

and for a coefficient $\eta = 1.44$ the real pendulum swings without reaching the angles of $\theta < 0.175[rad]$ or $\theta > 6.125[rad]$, as figure 5.9 shows.
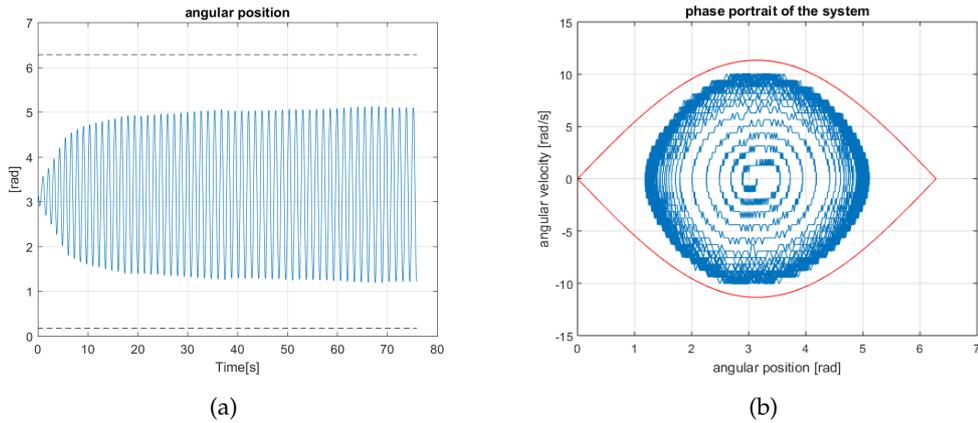
Figure 5.9: Real system response for the control law (5.3) and coefficient $\eta = 1.44$

Still, the applied motor force (F_M) is not enough to perform a complete swing up motion in order to place the pendulum in the operational range of the linear controller. Considering also that the applied control (5.3) contains both terms u and v, the bad response of the system may be related with the values of the terms u, v. Therefore, an analysis based on the simulation was performed investigating the ratio ($\frac{v}{u}$).

Figure 5.10 states the simulated evolution of the terms u,v for the applied control law (4.27) during the swing up control of the system.
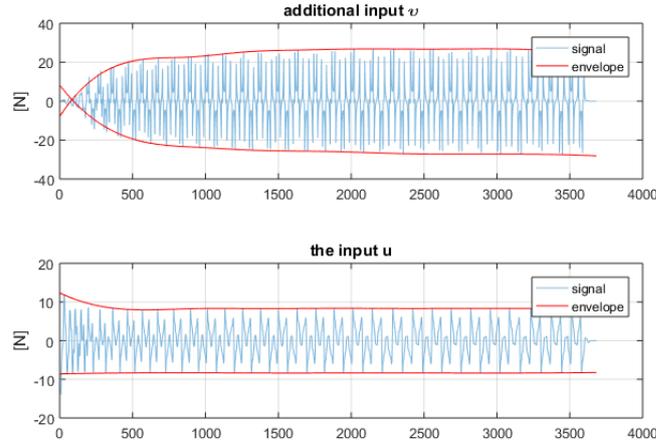
Figure 5.10: The terms of the theoretical control law (4.27).

Taking the peak envelopes for each signal it is approximated an average ration of

$$\frac{v}{u} \approx 4 \tag{5.4}$$

Apparently, with the usage of the control law (5.3) and a coefficient $\eta = 1.44$, the ratio $\frac{v}{u}$ is not close to 4 as it should, but much larger since the coefficient η is only proportional to the term u.

Therefore, a new coefficient η_2 is introduced to maintain the ratio between terms u and v. As a result, the applied control law in the real system reached its final form

$$u_{tot} = \eta \left(\underbrace{\frac{(-K_\delta \dot{x} - K_x x)\beta(q) - K_v \alpha(q, \dot{q})}{\beta(q)K_E E + K_v}}_{u} \right) + \eta_2 \left(\underbrace{sat\left(\frac{v}{v_{max}}, \frac{1}{v_{max}}\right)}_{v} \right) \tag{5.5}$$

Based on (5.4) and the already used coefficient $\eta = 1.44$, the new coefficient η_2 was estimated as

$$\eta_2 = \frac{\eta}{4} \Rightarrow \eta_2 = \frac{1.44}{4} \Rightarrow \eta_2 = 0.36 \tag{5.6}$$

Implementation and Validation of the Control Law

Finally, for the applied control law (5.5), where $\eta = 1.44$ and $\eta_2 = 0.36$ the physical inverted pendulum has the desired behaviour with a proper swinging and stabilization from the linear controller as it is demonstrated in figures 5.11 and 5.12.
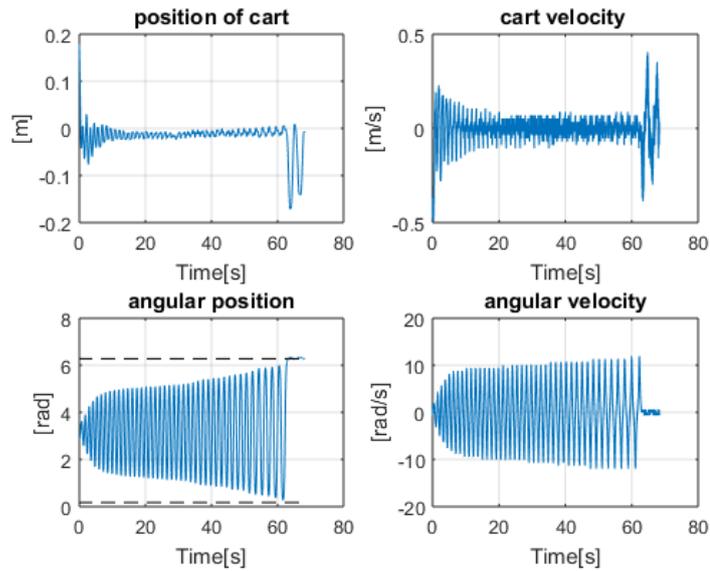
Figure 5.11: System response, using the control law (5.5) with coefficients $\eta = 1.44$ and $\eta_2 = 0.36$

(a)   (b)
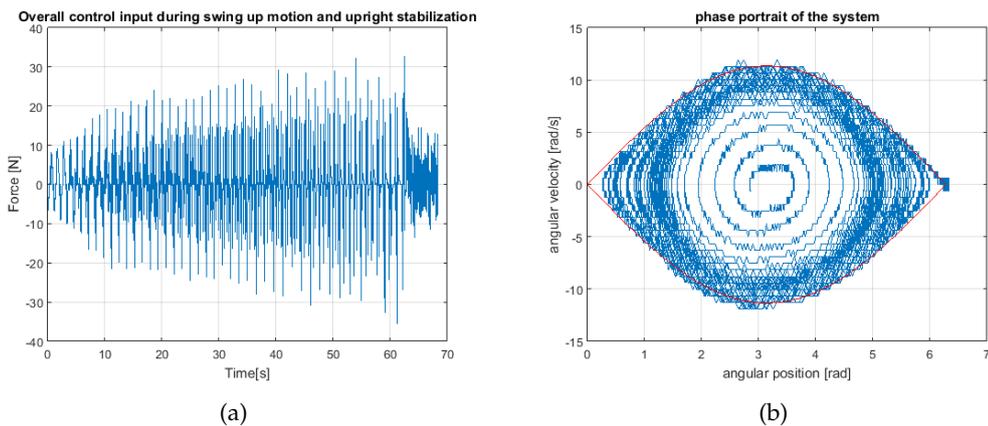
Figure 5.12: The overall applied control input and the corresponding phase portrait for the system. The control law (5.5) with coefficients $\eta = 1.44$ and $\eta_2 = 0.36$ is applied in the system only during the swing up motion $(0 - 63[s])$

The response of the real system is quite similar with the simulated one as it is demonstrated in figures 5.13, 5.14. The pendulum in both, simulation and reality, swings and is stabilized upright vertically at around 63[s].

Furthermore, it is validated the estimated coefficients η, η_2 as well as the form of the applied control law (5.5) in the physical system, since the graphs of angular displacement and velocity are quite similar.
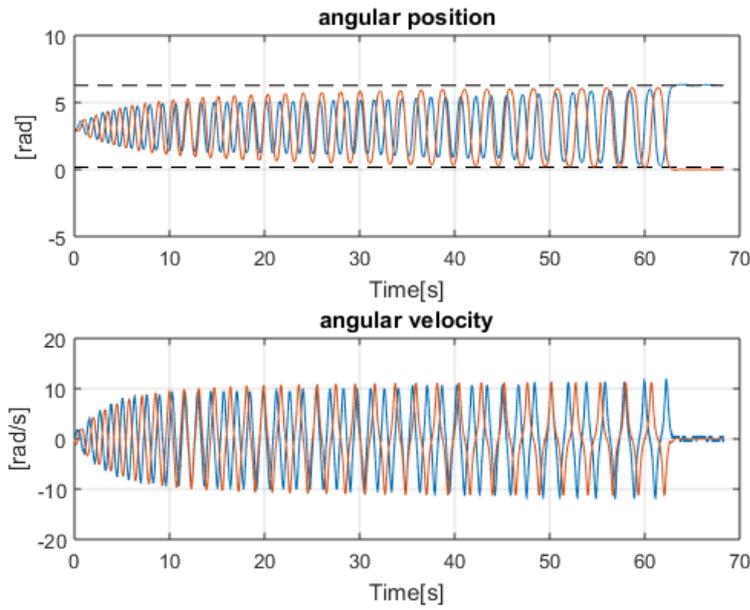
Figure 5.13: Real (blue) and simulated (red) system response for the applied control laws (5.5) and (4.27) respectivaly.

(a)   (b)
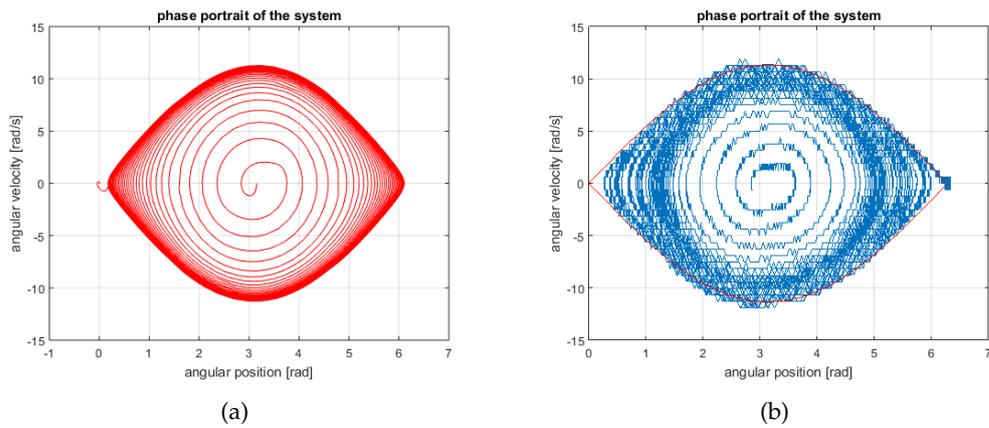
Figure 5.14: The phase portraits plots for the real (blue) and simulated (red) system response for the applied control laws (5.5) and (4.27) respectivaly.

In the simulation the swing up control switches to the linear one for an angle of $\theta < 0175[rad]$, while in reality for an angle $\theta > 6.125[rad]$. This is not an issue and is related only with estimated values of the system states$(x, \theta, \dot{x}, \dot{\theta})$ from the Matlab software.

In figure 5.15 the comparison between the energy level of the experimental data

and the simulated one (from figure 4.1) is presented. They confirm the expectations from the analysis with simulations in the previous chapter.
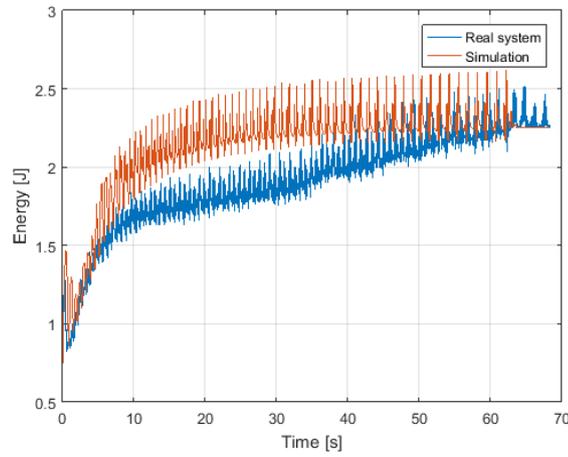
Figure 5.15: Energy of the real system (blue) and simulated one (red)

Chapter 6

States Estimation

Introduction

When using modern control theory, it is required to measure the states of a dynamical system in order to control it. This task is performed via sensors. Unfortunately in complex systems it is common that some of the system states are not measured directly from sensors. Moreover, some sensors give noise measurements making the system data collection and process a challenging task. This undesired situation is addressed by using state estimators that predict the unknown or uncertain states of a system. Kalman filters are state estimators based on stochastic models. These stochastic models describe noise characteristics (i.e. standard deviation, variance) of measured sensors data. In the control theory, this noise may be related with an uncertainty which had not been considered during the control design of a system. Kalman filter is a mathematical tool that makes optimal estimations using a system and a measurement model.

In the present chapter the objective is to perform state estimations using the model of the system presented in section 3.3. The available encoders measure the angular and the linear displacement of the system. In contrast, the angular and linear velocities $(\dot{x}, \dot{\theta})$ of the inverted pendulum are not measured directly from a sensor but initially they are estimated from the measured displacements according to:

$$\dot{\theta} = \frac{\Delta\theta}{T_s}, \quad \dot{x} = \frac{\Delta x}{T_s} \tag{6.1}$$

where T_s is the sampling time of the obtained data.

Therefore, the states $\dot{x}, \dot{\theta}$ may not be well estimated at first. Furthermore, all the measured states $(x, \theta, \dot{x}, \dot{\theta})$ may include an uncertainty due to a noisy signal. With a Kalman filter, optimal as well as less noisy estimations for the unknown and

known states of a system are obtained. In [3], [6] a Kalman filter is used for the state estimation of a mobile inverted pendulum such that to improve its balancing control. In the present thesis an extended Kalman filter is used in order to obtain more accurate states and improve the non linear swing up control of the system as well as its balancing control by the linear controller.

The difference between a Kalman filter (KF) and an extended Kalman filter (EKF) is that the first one is a linear estimator while the second a nonlinear estimator. The main parts of the present chapter are:

- Theoretical principle of the extended Kalman filter

- Design of the extended Kalman filter

- Results from the implementation of the extended Kalman filter in the real system

Extended Kalman Filter

Noise that is included in measured data is a parameter that is taken into account from both Kalman and extended Kalman filters. This noise is considered as white and consist of the system (w) and the measurement (v) noise [8]. In the KF the linear system and measurement equations are:

$$x = \mathbf{A}x + \mathbf{B}u + w$$
$$y = \mathbf{C}x + v \tag{6.2}$$

and for the EKF the non linear system and measurement equations are:

$$\dot{x} = f(x, u) + w$$
$$y = h(x) + v \tag{6.3}$$

Algorithm of Extended Kalman Filter

The EKF algorithm is implemented in discrete time. Therefore, the nonlinear system and measurement model in discrete time are presented.

$$x_{k+1} = f_d(x_k, u_k) + w_k, \quad w_k \sim \mathcal{N}(0, \mathbf{Q_k})$$
$$y_k = h_d(x_k, u_k) + v_k, \quad v_k \sim \mathcal{N}(0, \mathbf{R_k}) \tag{6.4}$$

where

x_k	the state vector of the system at time k
$f_d(x_k, u_k)$	the discrete non linear system equation
y_k	the output vector of the system at time k
$h_d(x_k, u_k)$	the discrete non linear measurement equation
$\mathcal{N}(\mu, \sigma^2)$	a Gaussian distribution with mean μ and covariance σ^2
w_k	the system noise with 0 mean and covariance $\mathbf{Q_k}$
$\mathbf{Q_k}$	the noise covariance matrix of the system
v_k	the measurement noise with 0 mean and covariance $\mathbf{R_k}$
$\mathbf{R_k}$	the noise covariance matrix of the measurement

An EKF deals with nonlinearities by linearizing the system during the actual estimation, and filters this linearized system via a KF. For this reason the system and measurement equations (6.4) are linearized by using partial derivatives with respect to the most recent estimations of x:

$$\mathbf{F_k} = \left.\frac{\partial f_d(x, u)}{\partial x^T}\right|_{\hat{x}_{k|k}, u_k} \qquad \mathbf{H_k} = \left.\frac{\partial h_d(x, u)}{\partial x^T}\right|_{\hat{x}_{k|k-1}, u_k} \tag{6.5}$$

where $\hat{x}_{k|k}$ is defined the estimation of the state x_k using known data at time k and $\hat{x}_{k|k-1}$ the estimation of the state x_k using known data at time $k - 1$. The EKF algorithm consists of 3 steps:

- **Initialization**

- **Prediction**

- **Time update**

Initialization: The predicted state $\hat{x}$ and the covariance matrix $\mathbf{P}$ of the state estimations are initialized:

$$\hat{x}_{0|-1} = 0$$
$$\mathbf{P}_{0|-1} = \mathbf{Q}$$

Prediction: At the current time k prediction is performed. Available actual measurements y_k, u_k are compared with previous state estimations and then corrected:

$$\hat{y}_{k|k-1} = h_d(\hat{x}_{k|k-1}, u_k)$$
$$\tilde{y}_{k|k-1} = y_k - \hat{y}_{k|k-1}$$
$$\mathbf{K_k} = \mathbf{P}_{k|k-1}\mathbf{H}_k^T(\mathbf{H}_k\mathbf{P}_{k|k-1}\mathbf{H}_k^T + \mathbf{R}_k)^{-1}$$
$$\hat{x}_{k|k} = \hat{x}_{k|k-1} + \mathbf{K}_k\tilde{y}_{k|k-1}$$
$$\mathbf{P}_{k|k} = (\mathbf{I} - \mathbf{K}_k\mathbf{H}_k)\mathbf{P}_{k|k-1}(\mathbf{I} - \mathbf{K}_k\mathbf{H}_k)^T + \mathbf{K}_k\mathbf{R}_k\mathbf{K}_k^T$$

Time update: From the time k to $k + 1$. The next state $\hat{x}$ and covariance matrix **P** are predicted:

$$\hat{x}_{k+1|k} = f_d(\hat{x}_{k|k}, u_k)$$
$$\mathbf{P}_{k+1|k} = \mathbf{F_k}\mathbf{P}_{k|k}\mathbf{F}_k^T + \mathbf{Q}_k$$

where

$\hat{y}_{k|k-1}$	the predicted measurement at time k, using the state prediction $\hat{x}_{k|k}$ made at time $k-1$
$\tilde{y}_{k|k-1}$	the measurement error at time k
$\mathbf{K_k}$	the Kalman gain at time k
$\hat{x}_{k|k}$	the state prediction at time k corrected from the kalman gain and the previous state estimation
$\mathbf{P}_{k|k}$	the covariance matrix of the state predictions at time k
$\hat{x}_{k+1|k}$	the updated state prediction corrected from the kalman gain and the actual state estimation made at time k
$\mathbf{P}_{k+1|k}$	the updated covariance matrix of the state predictions

The main concept in the EKF is to predict the prior state in the prediction step and update it in the update step, using the non linear model. This is performed by computing the kalman gain (K) and the covariance matrix (P) by using the linearized terms F_k, H_k of the non linear system (6.4).

Design of Extended Kalman Filter

Improvement in the control of the inverted pendulum is expected by the usage of an EKF which will process all the states of the system. More specifically, the states of the system are defined as:

$$\bar{x} = \begin{bmatrix} x \\ \theta \\ \dot{x} \\ \dot{\theta} \end{bmatrix} = \begin{bmatrix} x_1 \\ x_2 \\ x_3 \\ x_4 \end{bmatrix} \begin{matrix} \text{(cart horizontal position)} \\ \text{(pendulum angular position)} \\ \text{(cart horizontal velocity)} \\ \text{(pendulum angular speed)} \end{matrix} \qquad (6.6)$$

The model of the inverted pendulum presented in subsection 4.3.1 is:

$$(M+m)\ddot{x} - ml\dot{\theta}^2 \sin\theta + ml\ddot{\theta}\cos\theta = u$$
$$ml^2\ddot{\theta} - mgl\sin\theta + ml\cos\theta\ddot{x} = \gamma_r\dot{\theta} \tag{6.7}$$

and by introducing the notation (6.6) the nonlinear state equations of the system are obtained:

$$\dot{x}_1 = x_3$$
$$\dot{x}_2 = x_4$$
$$\dot{x}_3 = \frac{m\sin x_2(lx_4{}^2 - g\cos x_2) + \frac{\gamma_r\cos x_2 x_4}{l} + u}{M + m\sin^2 x_2}$$
$$\dot{x}_4 = \frac{-m^2l^2\sin x_2\cos x_2 x_4{}^2 - (M+m)\gamma_r x_4 + (M+m)gml\sin x_2 - ml\cos x_2 u}{ml^2(M + m\sin^2 x_2)} \tag{6.8}$$

where the form of the model is simplified by redefine the $\dot{x}_3$ as:

$$\dot{x}_3 = \frac{m\sin x_2(lx_4^2 - g\cos x_2) + \frac{\gamma_r\cos x_2 x_4}{l} + u}{M + m\sin^2 x_2} = \frac{\alpha(x_2, x_4) + u}{\beta(x_2)}$$

In this way. the nonlinear state equations for the system are:

$$\dot{x}_1 = x_3$$
$$\dot{x}_2 = x_4$$
$$\dot{x}_3 = \frac{\alpha(x_2, x_4) + u}{\beta(x_2)}$$
$$\dot{x}_4 = \frac{g}{l}\sin x_2 - \frac{\gamma_r x_4}{ml^2} - \frac{1}{l}\cos x_2\left(\frac{\alpha(x_2, x_4) + u}{\beta(x_2)}\right) \tag{6.9}$$

Since the displacements x_1, x_2 are the measurements from the physical system that are fed in the EKF, the measurement equations of the system are:

$$\begin{bmatrix} y_1 \\ y_2 \end{bmatrix} = \underbrace{\begin{bmatrix} 1 & 0 & 0 & 0 \\ 0 & 1 & 0 & 0 \end{bmatrix}}_{\mathbf{H}} \begin{bmatrix} x_1 \\ x_2 \end{bmatrix} \tag{6.10}$$

The models (6.8) and (6.10) are the system and the output model respectively, that are used from the EKF. In our system they have a continuous form:

$$\dot{\bar{x}} = f(\bar{x}, u)$$
$$y = \mathbf{H}\bar{x} \tag{6.11}$$

where the system model is nonlinear while the output model is linear. The system (6.11) should be discretized using the forward Euler method, since the algorithm of the EKF is referred in discrete time:

$$x_{k+1} = x_k + T_s f(x_k, u_k)$$
$$y_k = \mathbf{H} x_k \qquad (6.12)$$

with $T_s = 0.005[s]$ the used sampling time of the Arduino board, that is also used in the algorithm of the EKF. Consequently, the discrete form of the model (6.9) is:

$$x_{1k+1} = x_{1k} + T_s x_{3k}$$
$$x_{2k+1} = x_{2k} + T_s x_{4k}$$
$$x_{3k+1} = x_{3k} + T_s \frac{\alpha(x_{2k}, x_{4k}) + u}{\beta(x_{2k})}$$
$$x_{4k+1} = x_{4k} + T_s \left(\frac{g}{l} sinx_{2k} - \frac{\gamma_r x_{4k}}{ml^2} - \frac{1}{l} cosx_{2k} \left(\frac{\alpha(x_{2k}, x_{4k}) + u}{\beta(x_{2k})} \right) \right) \qquad (6.13)$$

As it was described in subsection 6.2.1 the derivation of the Kalman filter is used by the EKF in order to linearize the nonlinear terms only when it is needed. Therefore, it is convenient to present the discrete linearized system and output matrices of the system:

$$\mathbf{F_k} = \left. \frac{\partial f_d(x_k, u_k)}{\partial \bar{x}} \right|_{x_k, u_k} \qquad \mathbf{H_k} = \left. \frac{\partial h_d(x_k, u_k)}{\partial \bar{x}} \right|_{x_k, u_k} \qquad (6.14)$$

where H_k is defined in (6.10) and the state transition matrix F_k is given by:

$$\mathbf{F_k} = \mathbf{I} + T_s \left. \frac{\partial f(\bar{x}, u)}{\partial \bar{x}^T} \right|_{\hat{x}_{k|k}, u_k} \qquad (6.15)$$

Design of Measurement and System Noise

White noise is present in real world systems. Therefore, in the outputs of the sensors it is common to consider a white noise component, which has Gaussian distribution with zero mean $\mathcal{N}(0, \sigma^2)$ and random samples uncorrelated. In the Kalman theory the covariance matrices are expressed as $\mathbf{Q}$ for the system noise and as $\mathbf{R}$ for the measurement noise. These covariance matrices are the tuning parameters of the EKF since they affect the state estimations, as it can be seen from the EKF algorithm in subsecton 6.2.1.

Measurement noise

The state measurements of the investigated system are obtained trough quadrature encoders. Generally these type of sensors are very accurate with very small noise measurement. Initially, an attempt to detect a possible measurement noise was performed by observation of the sensors data when the system was not moving. However noise was measured. Afterwards considering that the sensors data comes from discrete measurements ($T_s = 0.005[s]$), the resolution of them was considered to define the measurement noise. Section 2.6 contains the approximated resolutions for the used encoders. These values can be referred as the standard deviations (σ) of the noise and from them the variance of the noise can be obtained as follows:

- The resolution of the encoder which measure the linear cart displacement is $Res_{cart} = 8 * 10^{-6}[m]/count \Rightarrow \sigma_{cart} = 8 * 10^{-6}[m]$. Therefore the cart measurement variance is defined as: $Var_{cart} = \sigma_{cart}^2 = 6.4 * 10^{-6}[m^2]$.

- The resolution of the encoder which measure angular pendulum displacement is $Res_{Pen} = 0.0031[rad]/count \Rightarrow \sigma_{pen} = 0.0031[rad]$. Thus, the pendulum measurement variance is defined as: $Var_{pen} = \sigma_{pen}^2 = 9.61 * 10^{-6}[rad^2]$.

Encoders data for the cart x and pendulum θ displacements are used during the design of the EKF. For this reason the covariance matrix **R** is square with dimensions $[2x2]$ defined as:

$$\mathbf{R} = \begin{bmatrix} R_x & 0 \\ 0 & R_\theta \end{bmatrix} = \begin{bmatrix} 6.4 * 10^{-6} & 0 \\ 0 & 9.61 * 10^{-6} \end{bmatrix} \tag{6.16}$$

The matrix **R** remains constant during the tuning process.

System Noise

The various components in the inverted pendulum system introduce noise during their operation. Moreover, external factors considered as uncertainties may also cause noise in the system. Therefore, the system noise is difficult to be measured. However, it can be estimated with values that correspond to Gaussian distributions. Also tuning is required to obtain good estimations. In the present thesis the system noise covariance matrix **Q** is defined as:

$$\mathbf{Q} = \begin{bmatrix} Q_x & 0 & 0 & 0 \\ 0 & Q_\theta & 0 & 0 \\ 0 & 0 & Q_{\dot{x}} & 0 \\ 0 & 0 & 0 & Q_{\dot{\theta}} \end{bmatrix}$$

since estimations for all the system states are obtained from the EKF algorithm .
Initially all variances have the same value (0.1) but after a simulation tuned process
the following covariance matrix **Q** was defined:

$$\mathbf{Q} = \begin{bmatrix} 0.01 & 0 & 0 & 0 \\ 0 & 0.1 & 0 & 0 \\ 0 & 0 & 100 & 0 \\ 0 & 0 & 0 & 10 \end{bmatrix} \tag{6.17}$$

An initial idea related with the variance values of **Q** was that the Q_x may have the
smallest value since it is the state of the system that is controlled directly from the
dc motor.

EKF Results

The EKF algorithm was tested and tuned in Matlab by using real system data. A guideline in the tuning process was that the state estimations should follow the real used measurements removing a possible noise at the same time. Also, the autocorrelation function (ACF) of error for the outputs x, θ was investigated. Ideally, the error should be uncorrelated.The results for the EKF estimations for the used covariance matrices (6.17) and (6.16) are presented below. Moreover figure 6.5 presents the applied control input in the system during the swing up motion and the linear control.

The estimated states for the linear and angular position of the system are quite similar with the real measured as it shows figure 6.1. The measured data seems without noise and the same trend is followed by the estimated data.
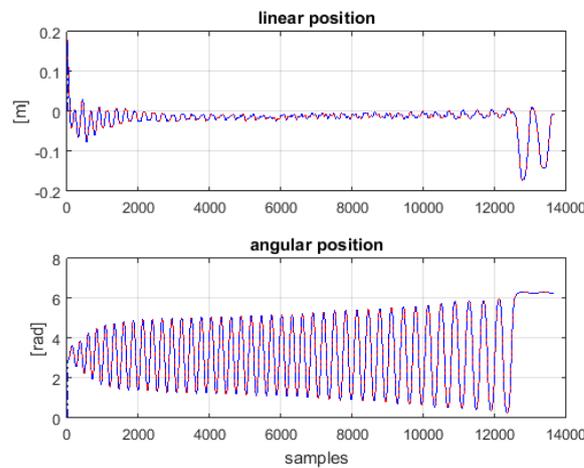
Figure 6.1: EKF estimated linear and angular positions (blue) and measured linear and angular positions (red)

On the other hand, figure 6.2 demonstrates a small estimation error for the linear and angular velocities. This variation may be due to the fact that for the state estimations, measured data for the linear and angular displacement are only used. The red graph in this figure corresponds to the estimated velocities from the numerical differentiation of the measured displacements. The purpose of the EKF was to improve these estimated velocities.

As shows figure 6.2 the EKF results (blue one) are less noise compared with the estimations made from the numerical differentiation of positions (red). This is more obvious during the linear control of the system as it is presented in figure 6.3

.
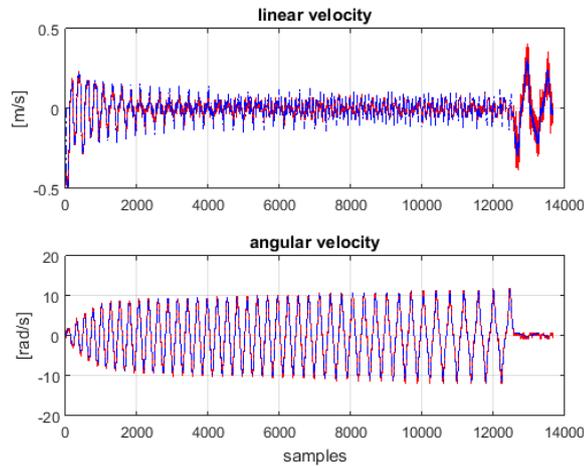
Figure 6.2: The estimated linear and angular velocities from the EKF (blue) and from the numerical differentiation of the measured positions (red)
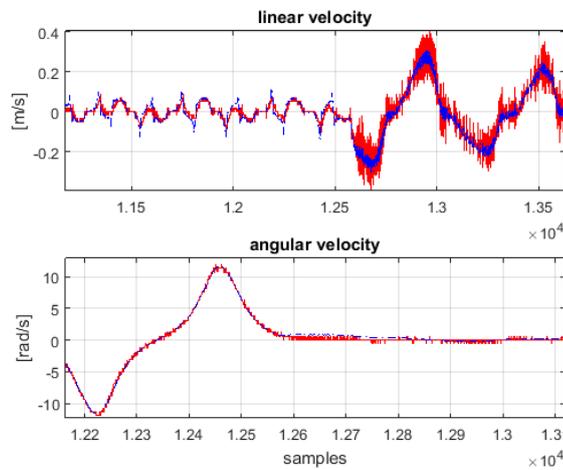
Figure 6.3: Zommed area of the system response shown in figure 6.2. Estimations of EKF (blue) and the numerical differentiation of the measured positions (red)

The autocorrelation functions of the linear (x) and angular (θ) position estimation error are almost 0 after the first time lag as it is shown in figure 6.4. Therefore, the filtered error is characterized as uncorrelated.
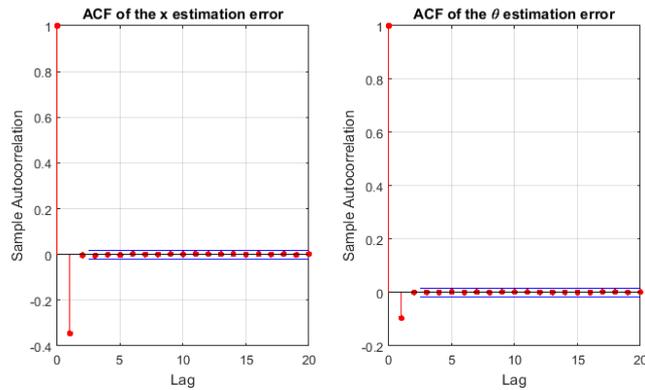
Figure 6.4: Autocorrelattion function for the estimated errors of cart(x) and pendulum(θ displacements)

Finally, the applied control input of the system is more steady especially during the linear control as shows figure 6.5. More specifically, without using the estimated states of the EKF the applied input is characterized by rapid fluctuations between $15[N]$ and $-15[N]$. By using the EKF estimations the applied control input had smaller and slower variations.
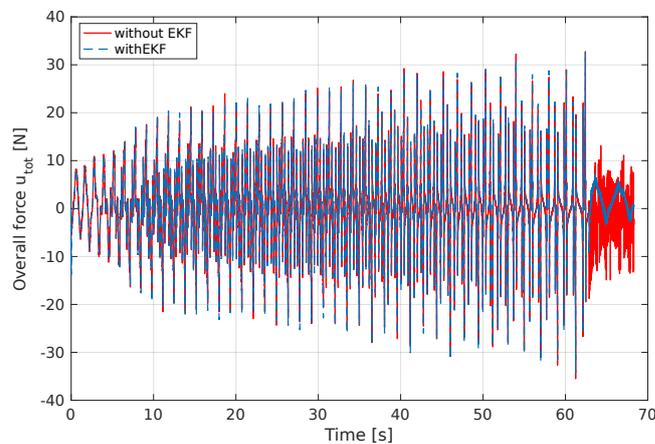
Figure 6.5: Applied control input in the system based on measured state values (red) and on EKF estimated state values (blue)

A stable DC motor operation can reduce the fatigue and increase the life span of this component. Moreover the energy demands of the device may be smaller.

The benefits of such a motor response can be considerable in terms of maintenance and energy consumption cost.

Summarizing, using state estimations from an EKF a different system response is observed. Less noise signals especially for the states of velocities during the linear control are observed. In practise, that may create a smoother motion of the system that may be valuable for specific applications. This result is supported also from the progression of the energy in figure 6.6
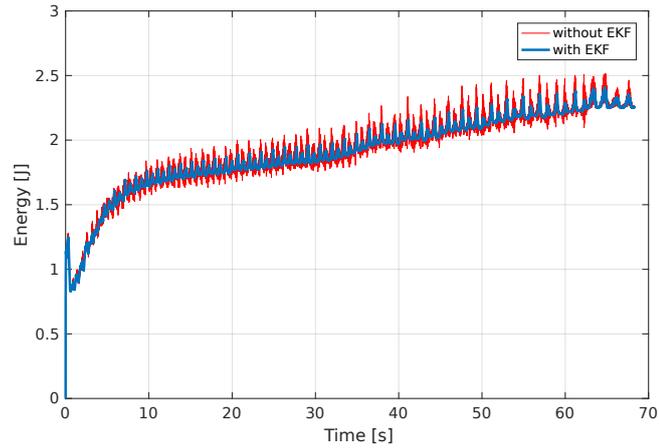
Figure 6.6: Energy of system using the measured states (blue) and the EKF estimated states (red)

Chapter 7

Conclusion

The classical system of the inverted pendulum is studied in this thesis. The absolutely main goal of balancing the pendulum upright starting from its downwards vertical position has been addressed. Lagrangian mechanics were used for the formulation of the inverted pendulum model. The available system, in the AAU laboratory facilities, consists of a mechanical and an electrical part. Dynamical analysis for each part was performed aiming to a more accurate model formulation. Results revealed that the effect of the electrical set up in the control of the system is inconsiderable.

The used non linear control strategy was based on an energetic approach of the system. Lyapunov theory was used for the derivation of the control law that swings up the pendulum from its hanging position. Close to the upright vertical position of the pendulum, the non linear control of the swinging motion switches to a linear one, designed at [4], in order to balance the pendulum. Through simulations, the inability of the non linear controller for an upswing motion was detected. Additional energy should be introduced in the system but precisely in order to create ideal situations for the linear control. A pendulum with the less possible angular velocity close to its upright position is a requirement for a successful linear control. Modifications in the designed swing up control law were based on the friction forces acting on the system during its motion. Moreover, a transition region which ensures a smooth control switching was developed through these modifications. The new obtained control law resulted to a successful swing up and balancing motion of the pendulum.

Difficulties during the implementation of the designed control in the physical system were present. In contrast with the good simulation results, the real system could not perform the complete task of the swing up and pendulum balance. Possible estimation errors between the unknown estimated system parameters and

the real one could be reasonable. Furthermore, model uncertainties that were not considered in the system dynamics could also be a factor for an undesired system response. To face this problem two scaling factors were introduced in the applied control that executes the swing up motion. In this way, the applied force in the cart of the system was regulated without changing the form of the applied control. The values of these factors were set via a tuning procedure which is presented in Chapter 5. Eventually, the real system performed a complete pendulum swing up and upright stabilization motion.

For the control of the system the feedback signals of the cart and pendulum positions and velocities are used. Noticeable noise was observed in the velocity measurements due to numerical differentiation. Therefore, an extended Kalman Filter (EKF) algorithm was used to perform state estimations. The resolution of the system sensors (encoders) were considered as a possible measurement noise while the system noise was estimated with a Gaussian distribution with zero mean $\mathcal{N}(0, \sigma^2)$ and random samples uncorrelated. The estimated states of velocities are less noise. It can be said that this may result in a more smooth system motion. In this way, financial benefits can be obtained due to a lower DC motor operation and maintenance cost. The estimated states were implemented off-line in the system as it is presented in Chapter 6. However, since data from the real system was used for the state estimations, quite similar results are expected during the implementation in the real system.

Due to time limitation the EKF algorithm was not applied in the real system. For this reason, this can be a further improvement of this study, that may result in interesting conclusions and findings. Better estimation methods for the unknown parameters as well as the usage of friction models in the system dynamics can create a more accurate model and consequently a better control. Other control algorithms (i.e. sliding mode, Lyapunov redesign, Linear Quadratic Gaussian (LQG)) can also be tested and evaluated .

Bibliography

[1] Arduino.cc (2016). `https://www.arduino.cc/en/Main/ArduinoBoardDue`.

[2] AvagoTechnologies (2014). @online. `http://www.avagotech.com/cs/Satellite?pagename=AVG2%2FsearchLayout&locale=avg_en&Search=+HEDS-5540&submit=search`.

[3] Carlsson, B. and Örback, P. (2009). Mobile inverted pendulum control of an unstable process using open source real-time operating system.

[4] Catarinacci, F. and Kapnisakis, I. (2016). *Control of an inverted pendulum*.

[5] Chung, C. C. and Hauser, J. (1995). Nonlinear control of a swinging pendulum. *Automatica*, 31(6):851–862.

[6] Eide, R., Egelid, P. M., Stamsø, A., and Karimi, H. R. (2011). Lqg control design for balancing an inverted pendulum mobile robot. *Intelligent Control and Automatica*.

[7] Fantoni, I. and Lozano, R. (2002). *Non-linear Control for Underactuated Mechanical Systems*. Springer London.

[8] Grewal, M. S. and Andrews, A. P. (2008). *Kalman Filtering Theory and Practice Using MATLAB 3rd edition*. A.John Wiley and sons.

[9] Ishitobi, M., Ohta, Y., Nishioka, Y., and Kinoshita, H. (2004). Swing-up of a cart–pendulum system with friction by energy control. *Proceedings of the Institution of Mechanical Engineers, Part I: Journal of Systems and Control Engineering*, 218(5):411–415.

[10] Jackson, E. A. (1989). *Perspectives of nonlinear dynamics*. New York.

[11] Jensen, B. D.McLain, T. W. (2016). Meen 335: System dynamics. `http://twmclasses.groups.et.byu.net/lib/exe/fetch.php?media=483:335notes.pdf`.

[12] Khalil, H. K. (2002). *Nonlinear systems*. Prentice Hall.

[13] maxonmotor.nl (2009). 4q dc servoamplifier ads 50/10 @online. `http://www.maxonmotor.nl/medias/sys_master/8803609280542/201583-ADS-50-10-Operating-Instructions-En.pdf`.

[14] maxonmotor.nl (2015). Maxon motor 370356 re 50 200w @online. `http://www.maxonmotor.com/medias/sys_master/root/8816799055902/15-143-EN.pdf`.

[15] Olsson, H., Åström, K., Canudas de Wit, C., Gäfvert, M., and Lischinsky, P. (1998). Friction models and friction compensation. *European Journal of Control*, 4(3):176–195.

[16] @online (2016). Spinning knobs: Custom rotary encoders. `https://todbot.com/blog/2008/06/17/get-on-the-blinkm-bus-with-a-blinkm-cylon/comment-page-1/`.

[17] Spong, M. and Praly, L. (1996). *Control of Underactuated Mechanical Systems Using Switching and Saturation*.

[18] Åström, K.J.Furuta, K. (2000). Swinging up a pendulum by energy control. *Automatica*, 36(2):287–295.

[19] Vallieres, M. (2016). Homoclinic orbit. `http://www.physics.drexel.edu/~valliere/PHYS305/Duffing/Duffing_story/node5.html`.

[20] Wei, Q., Dayawansa, W., and Levine, W. (1995). Nonlinear controller for an inverted pendulum having restricted travel. *Automatica*, 31(6):841–850.

[21] Weisstein, E. W. (2016). Ramp function – from wolfram mathworld. `http://mathworld.wolfram.com/RampFunction.html`.

[Zaccarian] Zaccarian, L. Dc science, dynamic model control techniques.

Appendix A

Parameter Estimation and Linear Controller

As it was referred in chapter 1, in the present work results and conclusions reported at [4] provide vital knowledge for the investigating non linear system in order to perform the objectives of this project. The inverted pendulum set up shown in figure A.1,is located in the laboratory facilities of the AAU. Its main parts are the cart with a mass (M), the pendulum rod with length $l = 0.305[m]$ and the pendulum with a mass $m = 0.251[kg]$. While the cart moves horizontally in the rail, friction forces exist with a direction opposite to the cart displacement. Also, during the pendulum rotational motion a friction torque is applied to the system. The values of the parameters related with the referred frictions of the system were unknown, thus they have been estimated. Below they are presented the estimated values of each parameter with a short description for the corresponding estimation procedure of each. The following content is also presented in [4] with more details.

Linear Friction Terms

During the horizontal cart movement linear frictions F_f are generated, which are represented by the model

$$F_f = \gamma \dot{x} + F_c sign(\dot{x}) \tag{A.1}$$

where

- γ the coefficient of viscous friction

- $F_c sign(\dot{x})$ the Coulomb friction of the cart that will be referred as F_c for simplicity.
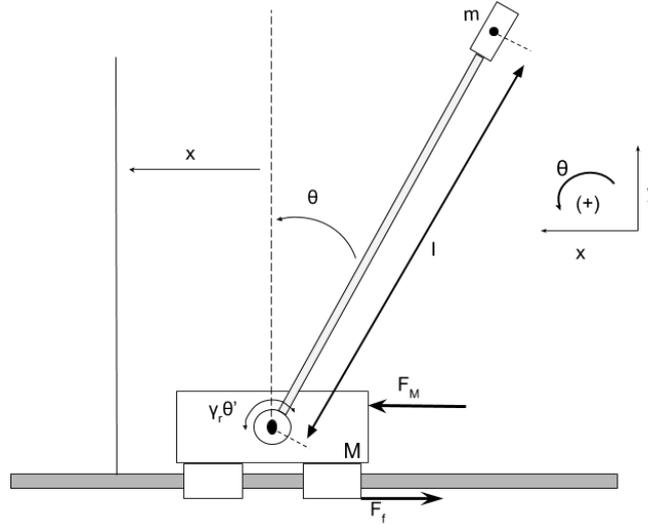
Figure A.1: The cart-pendulum system

- $\dot{x}$ the velocity of the pendulum cart, that is a state of the inverted pendulum system

The linearised model of the system (3.20), after a small-angle linearization ($\sin\theta \approx \theta$, $\cos\theta \approx 1$, $\dot{\theta}^2 \approx 0$) is defined as:

$$(M+m)\ddot{x} + F_f = F_M - ml\ddot{\theta} \tag{A.2a}$$

$$ml^2\ddot{\theta} = mgl\theta - ml\ddot{x} - \gamma_r\dot{\theta} \tag{A.2b}$$

Neglecting the pendulum mass (m) and its velocity ($\dot{\theta}$), and substituting (A.1) in (A.2a) it is obtained

$$M\ddot{x} + \gamma\dot{x} + F_c = F_M \tag{A.3}$$

which describes the cart motion of the inverted pendulum that will be used for the estimation of the γ coefficient. A signal that corresponds to a ramp function [21] was applied in the cart via the Arduino board that controls the DC motor which move the cart. In this way the cart moves with an almost constant velocity ($\ddot{x} = 0$). Thus the cart motion equation A.3 takes the form

$$\gamma\dot{x} + F_c = F_M \tag{A.4}$$

Due to the special construction characteristics of the inverted pendulum system it was found that there is a larger friction during the cart motion to the right side of the rail, compared with a motion to the left of the rail. Therefore two different estimations for the parameter γ and F_c were performed by using the same procedure.

The estimations of the Coulomb frictions (F_{c_L}, F_{c_R}) for a left and a right cart displacement were made considering equations (A.4), (A.1) as well as concepts related with the Coulomb friction (F_c) [15]. The friction, which resist to the motor force (F_M) and keeps the cart stationary, expresses the Coulomb friction F_c. Right before the cart starts moving, since its velocity is $(\dot{x} = 0)$ it exists $F_c = F_M$. Figure A.2 demonstrates one of the experimental tests of estimation.
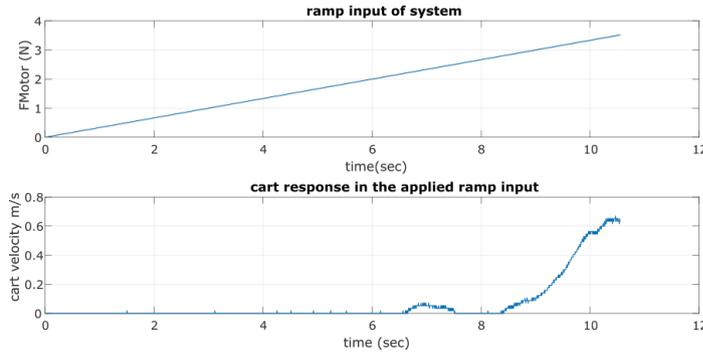
Figure A.2

The estimated Coulomb frictions were $F_{c_L} = 2.85[N]$, $F_{c_R} = 3.98[N]$ for a left and a right cart motion respectively. More details are presented at [4]

For a friction model consisted from Coulomb and viscous friction (A.1) the theoretical graph for the velocity of an object as function of its friction is shown in figure A.3. From the obtained data of the real system, it was constructed the experimental version of the figure A.3. The slope of the almost linear parts of the graphs that corresponds to the viscous friction $(\gamma \dot{x})$, represents the viscous coefficients (γ). Experimentally it was found $\gamma_R = 0.94$ for a right and $\gamma_L = 0.64$ for a left cart motion respectively, as it is also presented in [4].

Mass of the Cart

The mass of the cart (M) was estimated through the step response (figure A.4) of the system which was consisted only from the cart. Setting $F_M = 0$ from equation A.3 it is obtained

$$F_M = 0 \rightarrow \dot{v} = \frac{-\gamma v - F_c}{M} \tag{A.5}$$

that represent the response of the system when the control input is $u = 0$ (part after the time 0.2[s] in figure A.4) Solving A.5 with respect to M it is obtained

$$M = \frac{-\gamma v - F_c}{\dot{v}} \tag{A.6}$$
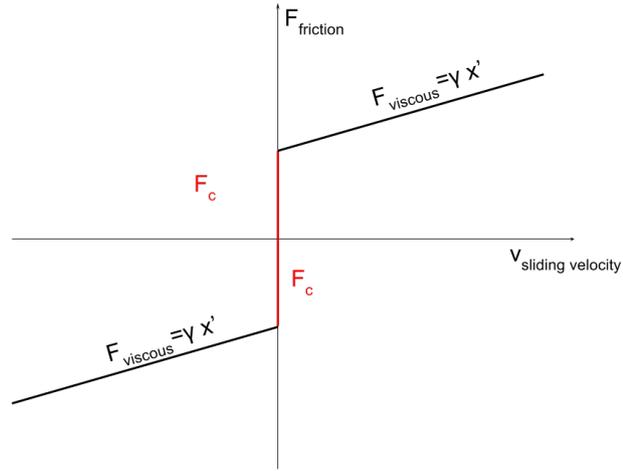
Figure A.3: Evolution of friction forces during the sliding motion of an object
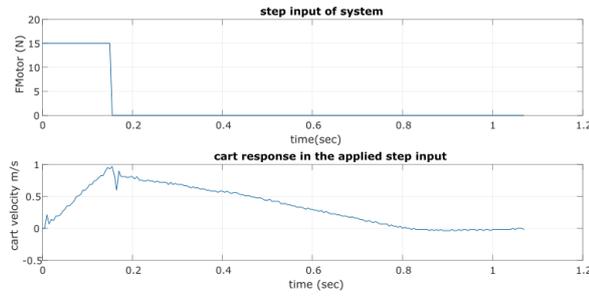
Figure A.4: Step input and corresponding response of the system.

Two estimations for the mass of the cart were performed, since the response of the system during a left and a right motion of the cart was different. The previous estimated parameters $(\gamma_R, \gamma_L, F_{c_R}, F_{c_L})$ were used for the cart mass estimation (M). Also, a data point (v, t) from the linear part of the system step response (figure A.5), gave the value of velocity in equation (A.6), while the acceleration is expressed from the slope of the graph in figure A.5.Following the same process for a left and right cart motion the two estimated masses were found $M_L = 2.357[kg]$, $M_R = 3.95[kg]$ while the final cart mass estimation

$$M = \frac{M_L + M_R}{2} = \frac{2.357 + 3.95}{2} = \textbf{3.15kg} \qquad (A.7)$$
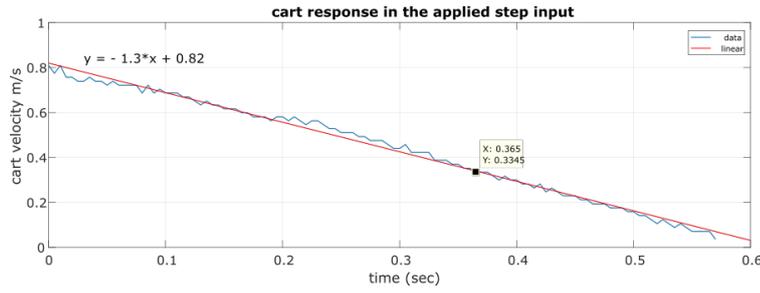
Figure A.5: The linear part of the systemm response in the step input.

Rotational Viscous Coefficient

During the pendulum motion, rotational friction ($\gamma_r \dot{\theta}$) is acting in the pendulum. Through a free pendulum motion, (starting from initial system states:$[x_0 \, \theta_0 \, \dot{x}_0 \, \dot{\theta}_0] = [0 \, -1.57rad \, 0 \, 0]$) and without any input in the system, an estimation for the rotational viscous coefficient γ_r was performed. During this movement the pendulum performs a damped sinusoidal motion (figure A.6) which can be upper and lower bounded from two exponential function ($e^{-\sigma t}$, $-e^{-\sigma t}$) where $\sigma = \omega_n \zeta$.
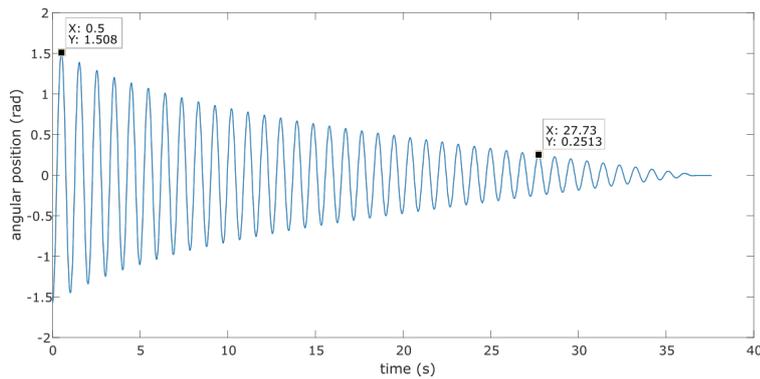
Figure A.6: Pendulum free motion response

The motion of a damped second order system like the pendulum is expressed by

$$\ddot{x} + 2\sigma \dot{x} + \omega_n^2 x = 0 \tag{A.8}$$

and relating (A.8) with

$$ml^2 \ddot{\theta} - mgl \sin \theta + ml \cos \theta \ddot{x} = -\gamma_r \dot{\theta}$$

which is the equation of the inverted pendulum model that expresses the motion of the pendulum, it is obtained

$$\frac{\gamma_r}{ml} = 2\sigma \Rightarrow \gamma_r = 2ml\sigma = 2ml\omega_n\zeta. \tag{A.9}$$

Through logarithmic decrement method [11] the system parameters σ, ζ, ω_d and ω_n are defined, considering two points from the pendulum free motion response (figure A.6). The found parameters were

- $\zeta = 0.00983$

- $\omega_d = 6.6914 [rad/s]$

- $\omega_n = 6.6981 [rad/s]$

whose calculations are presented analytically in [4].
Consequently, using A.9 is obtained $\gamma_r = 0.00983$. The exponential boundaries of the pendulum response are $\pm\theta_0 e^{-\sigma t} \Rightarrow \pm 1.57 e^{-0.0657t}$ which fits well to the damped sinusoidal motion of the pendulum as it is shown in figure A.7.
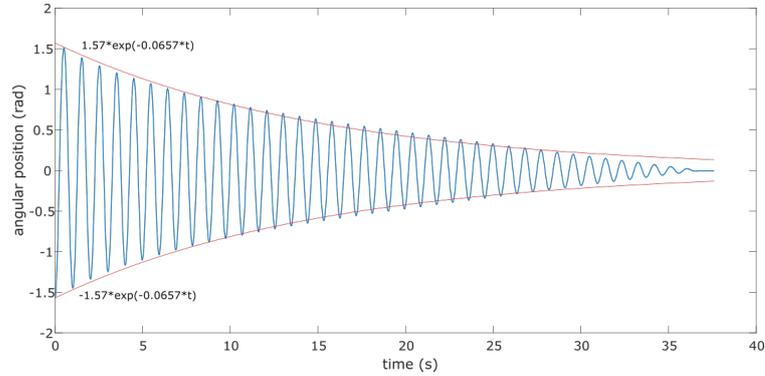
Figure A.7: Envelopes representing the decay of the pendulum free motion

Linear Controller

The pendulum of the system is stabilized upright vertically ($\theta = 0$) via a linear controller. This controller acts within the neighbour region of the unstable equilibrium point of the system ($\theta = 0$). For the design of the linear controller K_1 the linearized model (A.2) was used. Through small angle approximation the linear state space form of (A.2) is defined as:

$$\begin{bmatrix} \dot{x}_1 \\ \dot{x}_2 \\ \dot{x}_3 \\ \dot{x}_4 \end{bmatrix} = \underbrace{\begin{bmatrix} 0 & 0 & 1 & 0 \\ 0 & 0 & 0 & 1 \\ 0 & -\frac{mg}{M} & -\frac{\gamma}{M} & \frac{\gamma_r}{Ml} \\ 0 & \frac{M+m}{Ml}g & \frac{\gamma}{Ml} & -\frac{(M+m)\gamma_r}{mMl^2} \end{bmatrix}}_{\mathbf{A}} \begin{bmatrix} x_1 \\ x_2 \\ x_3 \\ x_4 \end{bmatrix} + \underbrace{\begin{bmatrix} 0 \\ 0 \\ \frac{1}{M} \\ -\frac{1}{Ml} \end{bmatrix}}_{\mathbf{B}} F_M$$

where

$$\begin{bmatrix} x \\ \theta \\ \dot{x} \\ \dot{\theta} \end{bmatrix} = \begin{bmatrix} x_1 \\ x_2 \\ x_3 \\ x_4 \end{bmatrix} \quad \begin{array}{l} \text{(cart horizontal position)} \\ \text{(pendulum angular position)} \\ \text{(cart horizontal velocity)} \\ \text{(pendulum angular speed)} \end{array}$$

From desired response characteristics, the poles of the linearized inverted pendulum were obtained:

$$-2 \pm 2.20j, \quad -4 \pm 4.4j$$

Using Ackerman's formula via command *(A,B,poles)* in the Matlab software the gain vector of the linear controller K_1 was obtained:

$$K_1 = \begin{bmatrix} -30.6130 & -121.4494 & -22.5738 & -17.1256 \end{bmatrix} \tag{A.10}$$

The method of pole placement was used to obtain the control gain vector $K_1 = \begin{bmatrix} -30.6130 & -121.4494 & -22.5738 & -17.1256 \end{bmatrix}$. The applied law for the linear control of the system was

$$u = K_1 * \begin{bmatrix} x & \theta & \dot{x} & \dot{\theta} \end{bmatrix} \tag{A.11}$$

An analytical description of this design procedure is also presented in [4].

Conversion Force Factor

The designed control input u corresponds to a proper force F_M which is applied in the cart of the physical system. A belt connects the shaft of the DC motor with the cart via a wheel as shows figureA.8.

In this way the produced torque of the motor applies the force F_M in the cart according to:

$$F_M = \frac{k_M * I_M}{r} \tag{A.12}$$

where,

- $k_M = 0.0934$ the motor torque constant as referred in [14]

- $r = 0.03[m]$ the radius of the used wheel for the connection of the DC motor to the cart via the belt

- I_M the applied current to the motor

A digital set point value is defined in the Arduino Due board according to a designed control input u. This reference value, referred with the variable `SetOutSled`
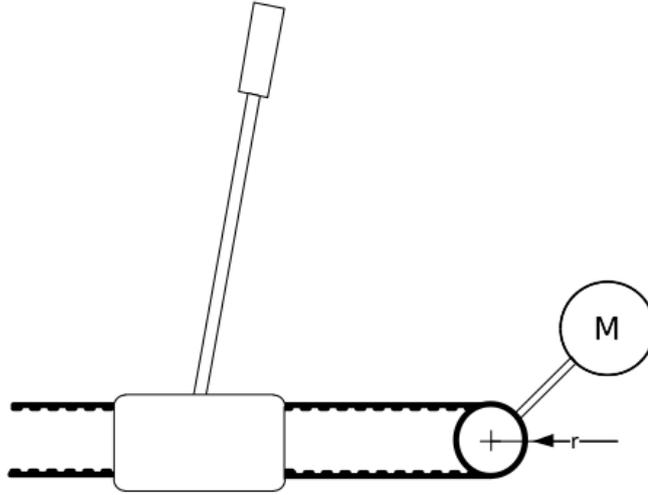
Figure A.8: DC motor-cart interconnection

in the Arduino code, is transformed, through a power amplifier, to a specific current I_M that supplies the DC motor. In [4] is presented a detail experimental process involving measurements in different points of the input system of the physical inverted pendulum. It was estimated that the current sent in the motor is proportional to the reference value by way of a coefficient b

$$I_M = b * \texttt{SetOutSled} \tag{A.13}$$

where $b = 0.00579$ defines the supplied current of the motor (I_M) according to the digital set value `SetOutSled` that is set in the Arduino code.

Considering that the force F_M is the applied control in the physical system that is defined from the reference value `SetOutSled` in the Arduino code, from (A.12), (A.13) is obtained

$$F_M = \frac{k_M * b * \texttt{SetOutSled}}{r} \Rightarrow \texttt{SetOutSled} = \frac{1}{\frac{k_M*0.00579}{0.03}} * F_M \tag{A.14}$$

where the term

$$\frac{1}{\frac{k_M*0.00579}{0.03}} = 55.47$$

is defined as the variable `Conv FM to u` in the Arduino code and determines the applied force (F_M) from the motor to the cart, according to the value `SetOutSled`.

A summary of the Appendix A content is presented via the table A.1

Table A.1: Estimated parameters

Parameters	
Coulomb friction for left cart displacement (F_{cL})	2.85N
Coulomb friction for right cat displacement (F_{cR})	3.98N
Viscous friction coefficient for left cart displacement (γ_L)	0.64
Viscous friction coefficient for right cart displacement (γ_R)	0.94
Mass of the cart (M)	3.15kg
Viscous rotational friction coefficient for pendulum (γ_r)	0.00983
Coefficient `Conv Fm to u`	55,47
Linear controller K_1	$[-30.6130, -121.4494, -22.5738, -17.1256]$